

THE AGE AND DISTANCE OF THE *KEPLER* OPEN CLUSTER NGC 6811 FROM AN ECLIPSING BINARY, TURNOFF STAR PULSATION, AND GIANT ASTEROSEISMOLOGY *

ERIC L. SANDQUIST¹; J. JESSEN-HANSEN²; MATTHEW D. SHETRONE³; KARSTEN BROGAARD^{2,4}; SØREN MEIBOM⁵; MARIKA LEITNER⁶; DENNIS STELLO⁷; HANS BRUNTT²; VICTORIA ANTOCI⁴; JEROME A. OROSZ¹; FRANK GRUNDAHL⁴; SØREN FRANDBSEN⁴

Draft version September 13, 2018

ABSTRACT

We present the analysis of an eccentric, partially eclipsing long-period ($P = 19.23$ d) binary system KIC 9777062 that contains main sequence stars near the turnoff of the intermediate age open cluster NGC 6811. The primary is a metal-lined Am star with a possible convective blueshift to its radial velocities, and one star (probably the secondary) is likely to be a γ Dor pulsator. The component masses are $1.603 \pm 0.006(\text{stat.}) \pm 0.016(\text{sys.})$ and $1.419 \pm 0.003 \pm 0.008 M_{\odot}$, and the radii are $1.744 \pm 0.004 \pm 0.002$ and $1.544 \pm 0.002 \pm 0.002 R_{\odot}$. The isochrone ages of the stars are mildly inconsistent: the age from the mass-radius combination for the primary ($1.05 \pm 0.05 \pm 0.09$ Gyr, where the last quote was systematic uncertainty from models and metallicity) is smaller than that from the secondary ($1.21 \pm 0.05 \pm 0.15$ Gyr) and is consistent with the inference from the color-magnitude diagram (1.00 ± 0.05 Gyr).

We have improved the measurements of the asteroseismic parameters $\Delta\nu$ and ν_{max} for helium-burning stars in the cluster. The masses of the stars appear to be larger (or alternately, the radii appear to be smaller) than predicted from isochrones using the ages derived from the eclipsing stars.

The majority of stars near the cluster turnoff are pulsating stars: we identify a sample of 28 δ Sct, 15 γ Dor, and 5 hybrid types. We used the period-luminosity relation for high-amplitude δ Sct stars to fit the ensemble of the strongest frequencies for the cluster members, finding $(m - M)_V = 10.37 \pm 0.03$. This is larger than most previous determinations, but smaller than values derived from the eclipsing binary (10.47 ± 0.05).

Keywords: binaries: eclipsing — binaries: spectroscopic — open clusters and associations: individual (NGC 6811) — asteroseismology — stars: variables: delta Scuti — stars: distances

1. INTRODUCTION

With the completion of a long stare at its original field, a host of new astrophysical information is available on

*BASED ON OBSERVATIONS MADE WITH WITH THE HOBBY-EBERLY TELESCOPE, WHICH IS A JOINT PROJECT OF THE UNIVERSITY OF TEXAS AT AUSTIN, THE PENNSYLVANIA STATE UNIVERSITY, STANFORD UNIVERSITY, LUDWIG-MAXIMILIANS-UNIVERSITÄT MÜNCHEN, AND GEORG-AUGUST-UNIVERSITÄT GÖTTINGEN; AND THE NORDIC OPTICAL TELESCOPE, OPERATED BY THE NORDIC OPTICAL TELESCOPE SCIENTIFIC ASSOCIATION AT THE OBSERVATORIO DEL ROQUE DE LOS MUCHACHOS, LA PALMA, SPAIN, OF THE INSTITUTO DE ASTROFISICA DE CANARIAS

¹San Diego State University, Department of Astronomy, San Diego, CA, 92182; esandquist@mail.sdsu.edu, jorosz@mail.sdsu.edu

²Stellar Astrophysics Centre, Department of Physics and Astronomy, Aarhus University, Ny Munkegade 120, DK - 8000 Aarhus C, Denmark; jjh@phys.au.dk, kfb@phys.au.dk, bruntt@gmail.com, antoci@phys.au.dk, fgj@phys.au.dk, srf@phys.au.dk

³University of Texas, McDonald Observatory, HC75 Box 1337-L Fort Davis, TX, 79734; shetrone@astro.as.utexas.edu

⁴Department of Physics & Astronomy, University of Victoria, P.O. Box 3055, Victoria, BC V8W 3P6, Canada

⁵Harvard-Smithsonian Center for Astrophysics, Cambridge, MA 02138; smeibom@cfa.harvard.edu

⁶Humboldt State University, Department of Physics & Astronomy, 1 Harpst St., Arcata, CA, 95521; rika.six@gmail.com

⁷Sydney Institute for Astronomy (SIfA), School of Physics, University of Sydney, NSW, 2006, Australia; stello@physics.usyd.edu.au

the star clusters observed during the original *Kepler* mission. Variable stars of many different types were discovered and studied thanks to the high-precision photometry and the nearly total coverage of the cycles of even long-period variables. One of the challenges in the aftermath of the *Kepler* mission continues to be the synthesis of information derived from large samples of stars.

Our focus in this paper is the sample of stars from one of the open star clusters in the original *Kepler* field. The brightest stars of the open cluster NGC 6811 comprise a rich set of objects with astrophysical information that has not yet been fully exploited. On the cool side, there are a group of helium-burning red clump and asymptotic giant stars with solar-like oscillations previously detected with the *Kepler* spacecraft (Stello et al. 2011a,b; Hekker et al. 2011; Corsaro et al. 2012). On the hot side, the bright end of the main sequence fits neatly within the instability strip, and δ Scuti (Sct) and γ Doradus (Dor) pulsating stars have been previously identified (van Cauteren et al. 2005; Luo et al. 2009; Debosscher et al. 2011; Uytterhoeven et al. 2011). This part of the color-magnitude diagram is known to contain chemically peculiar Am/Fm and Ap stars, although none has previously been identified in this cluster. With the rich set of information available for these kinds of stars, astrophysical information from one type of star will undoubtedly illuminate the others.

The main, but not the only, focus of the present paper is the brightest known eclipsing binary in the

cluster. The eclipsing binary KIC 9777062 ($\alpha_{2000} = 19^h37^m50^s.58$, $\delta_{2000} = +46^\circ35'23''.0$; also star 195 in Sanders 1971, and WEBDA 484) under consideration here was first identified in the *Kepler* Eclipsing Binary Catalog (Prša et al. 2011). *Kepler* observed this system almost continuously during the main mission, thanks to a special effort by the science team to study clusters (the *Kepler* Cluster Study; Meibom et al. 2011). Long-period eclipsing binary stars are treasures for stellar astrophysicists because they offer the chance to examine the characteristics of (effectively) isolated stars with a high degree of precision and accuracy. Mass and radius in particular can be simultaneously measured to precisions of better than 1% in many cases (Andersen 1991; Torres et al. 2010). When one or both of the stars in the binary has evolved significantly off of the zero-age main sequence and approaches the end of core-hydrogen burning, the radius becomes an age-sensitive quantity. And if the binary is a member of a star cluster, this gives us a means of tightly constraining the age of the cluster and testing stellar evolution theory quite strictly (e.g. Brogaard et al. 2012, 2011; Meibom et al. 2009).

Variability study of NGC 6811 began with van Cauteren et al. (2005) and continued with Rose & Hintz (2007) and Luo et al. (2009). Most variable star detections have been pulsating stars (like δ Sct) near the turnoff of the cluster, although two possibly eclipsing variables were discovered by van Cauteren et al.. Balona et al. (2011) examined variability for three early A-type stars in NGC 6811, including one that appeared to be a binary star.

As part of this paper, we have examined the photometry and membership of nearly all bright potential members of the cluster. This step is particularly important for a relatively sparse cluster like NGC 6811 because of the small number of stars in the more advanced stages of evolution. But even so, high quality photometry for the color-magnitude diagram (CMD) can nonetheless provide strong constraints on the age of the cluster and important physical effects influencing stars near the cluster turnoff. In §2, we describe the observational material we have gathered on the binary KIC 9777062 and other stars near the turnoff of NGC 6811. In §3, we present the analysis of the eclipsing binary KIC 9777062. In the discussion in §4, we describe the various observational constraints on the characteristics of NGC 6811, including the cluster’s distance and age.

1.1. Cluster Chemical Composition and Reddening

The chemical composition and reddening values for the cluster are important for the interpretation of many aspects of the work described here, so we will first summarize previous results from the literature and present one new determination of the reddening.

Until very recently, metallicity determinations have been indirect and not from spectroscopy. Molenda-Žakowicz et al. (2013) obtained high-resolution spectra of 5 cluster giants, and the average metallicity derived from these stars were $[\text{Fe}/\text{H}] = 0.00 \pm 0.02$ and $+0.01 \pm 0.04$ using two different abundance analysis algorithms. It is important to note that i) neither of these measurements employed asteroseismic $\log g$ measurements, and the average deviation of the measured $\log g$ from the as-

teroseismic values is about 0.5 dex for the second algorithm, and ii) the second of these measurements was differential with respect to solar abundances, whereas the remaining measurements described below are not. Molenda-Žakowicz et al. (2014) used medium-resolution ($R = 25000$) spectroscopy along with asteroseismic $\log g$ values for the observed giants to find an average of $[\text{Fe}/\text{H}] = +0.04 \pm 0.01$, where the quoted uncertainty does not include sources of systematic errors. (Three of the five giant stars they used overlapped with the 2013 sample.) Six cluster giants also have infrared spectroscopic abundances from the APOGEE survey (Data Release 12; Holtzman et al. 2015), which uses synthetic spectra (employing an Asplund et al. 2005 solar abundance mix) as comparisons. For these stars, the average metal content is $[\text{M}/\text{H}] = +0.05 \pm 0.02$, and iron abundance is $[\text{Fe}/\text{H}] = +0.02 \pm 0.02$. Frinchaboy et al. (2013) derived a value of $[\text{M}/\text{H}] = -0.02 \pm 0.04$ from APOGEE pipeline analysis of 2 members. Even with all of the caveats, the different spectroscopic measurements agree surprisingly well.

For our ultimate comparisons with models, however, we need to consider effects on the total metal mass fraction Z more carefully. The APOGEE project produces abundance measurements of the CNO elements that contribute about half of the metal content. For the six measured giant stars, the average abundances were $[\text{C}/\text{H}] = -0.12 \pm 0.02$, $[\text{N}/\text{H}] = +0.26 \pm 0.03$, and $[\text{O}/\text{H}] = +0.03 \pm 0.02$. Molenda-Žakowicz et al. (2014) found solar abundance ratios (with the exception of an overabundance of Ba) for 31 elements in 5 stars. Although the individual element differences with the Sun are potentially interesting, the CNO elements taken together imply only a small modification of the Z relative to the Sun. We will return to this discussion in Section 4.

Early studies of the cluster reddening used $E(B - V) = 0.16$, but more recent ones have shown evidence for a lower value. The galactic reddening map of Schlafly & Finkbeiner (2011) indicates that the integrated reddening along lines of sight through NGC 6811 should be $E(B - V)$ between 0.129 and 0.135, and this should be an upper limit for the cluster. The cluster reddening has been re-evaluated recently, although all of these newer studies effectively compare photometric data to isochrones and are therefore subject to a host of uncertainties, both theoretical (differences in the physics in the stellar models, and color-temperature transformations) and observational (such as the weighting of the contributions from the photometric sample). Three studies (Glushkova et al. 1999; Janes et al. 2013; Yontan et al. 2015) used *UBVRI* photometry to derive reddenings. Glushkova et al. (1999) found $E(B - V) = 0.12 \pm 0.02$ from fits of an older generation of isochrones to their *UBVRI* photometry in the CMD and two-color diagrams. Janes et al. (2013) derived $E(B - V) = 0.074 \pm 0.024$ from a Bayesian comparison of their *UBVRI* photometry with Yale-Yonsei and Padova isochrones in various CMDs. Yontan et al. (2015) derive $E(B - V) = 0.046 \pm 0.012$ from a Bayesian comparison of their *UBVRI* photometry with Padova isochrones in CMDs and two-color diagrams. Peña et al. (2011) determined $E(B - V) = 0.14$ from Strömgen photometry, but

their cluster member CMD has a large amount of scatter and they derive an unrealistically small age (about 190 Myr), so we do not believe this value is reliable. Molenda-Żakowicz et al. (2014) quote $E(B - V) = 0.05 \pm 0.02$ based on a comparison with PARSEC isochrones using spectroscopic T_{eff} and asteroseismic information.

To get an independent measure of the interstellar reddening $E(B - V)$ we exploited the calibration of the interstellar Na D line strength to $E(B - V)$ by Munari & Zwitter (1997). We measured the equivalent width W of the interstellar Na lines from the spectra of five cluster member giants obtained by Molenda-Żakowicz et al. (2014), subtracting in each case the contribution from the overlapping stellar Na lines by employing a template spectrum from Coelho et al. (2005) with stellar parameters close to those measured by Molenda-Żakowicz et al. (2014). To be exact, the parameters were $\log g = 3.0$, $[\text{Fe}/\text{H}] = 0.0$, and $T_{\text{eff}} = 5000$ K. We made use of both the D1 and D2 lines, and the wavelength ranges over which the equivalent width was measured were 5888.5 – 5890.8 Å and 5894.5 – 5896.9 Å, respectively. We used a factor of 1.1 to estimate $W(\text{D1})$ from $W(\text{D2})$ (see Munari & Zwitter 1997), and found agreement with the direct estimate of $W(\text{D1})$ for most stars at a level below 0.01 and never worse than 0.02. Averaging the results from the two lines and then from the 10 spectra (two of each star) yielded $W(\text{D1}) = 0.192 \pm 0.027$. Using the calibration in table 2 of Munari & Zwitter this resulted in $E(B - V) = 0.068 \pm 0.009$ where the uncertainty is the standard deviation of the mean. However, to account also for the uncertainty in the calibration we adopt $E(B - V) = 0.07 \pm 0.02$ as our reddening estimate. We note that Munari & Zwitter state a much larger uncertainty on the calibration, but we argue as in Brogaard et al. (2011) that the scatter around their calibration is very low at $E(B - V)$ values below 0.2 (see lower panel of their figure 4). As additional evidence, this method was used by Brogaard et al. (2011) to determine the reddening of the open cluster NGC 6791, producing a value in good agreement with other estimates. We will use $E(B - V) = 0.07 \pm 0.02$ as our primary choice when needed in the analysis below.

2. OBSERVATIONAL MATERIAL AND DATA REDUCTION

2.1. Kepler Photometry

Long cadence (30 min exposure time) data were recorded for KIC 9777062 during the entire 17 quarter duration of the main *Kepler* mission. In addition, short cadence (1 min exposure time) observations were taken during 6 different month-long periods within quarters 4, 10, and 14.

For our analysis we made use of light curves derived from the Pre-search Data Conditioning (PDC) pipeline (Stumpe et al. 2012; Smith et al. 2012) from Data Release 21, but we verified that these were good representations of the eclipses by comparing to our own reduction of the raw pixel data. The PDC pipeline cotrends light curves against those of other stars on the same CCD to identify and remove systematic trends (Kinemuchi et al. 2012), and also applies corrections to the flux measurements to account for contamination by other nearby stars. Although KIC 9777062 is in the field of NGC 6811, the cluster is a fairly sparse one and KIC 9777062 is well

Table 1
Photometric Observations at Mount Laguna Observatory
1-meter

UT Date	Filters	mJD ^a Start	N
2012 Jun. 2	VI_c	6080.71580	68,46
2012 Jul. 3	VI_c	6111.65676	77,75
2012 Jul. 22	VI_c	6130.66256	80,80
2012 Jul. 30	VI_c	6138.66063	42,49
2012 Aug. 26	BVI_c	6165.72618	5,5,5; calibration
2013 Jun. 14	BI	6457.68656	52,28
2013 Jul. 30	BI	6503.65531	67,26
2013 Aug. 9	BVI_c		calibration
2014 May 26	BV	6803.73965	40,21
2014 Jun. 22	BV	6830.68880	46,27
2014 Jul. 30	BV	6868.65135	47,48
2014 Aug. 11	BV	6880.65445	36,40

^a mJD = BJD - 2450000

outside the densest parts of the cluster. As a result, contaminating light from other stars is a relatively minor consideration: the contamination index (ratio of contaminating flux to total flux in the photometric aperture) from the *Kepler* Data Search at the Mikulski Archive for Space Telescopes (MAST; Brown et al. 2011) ranged from 0.007 to 0.014.

After some trials, we settled on the use of short cadence data in our analysis, largely for the greater time resolution. Five of the six months of short cadence data were also taken during the same *Kepler* observing season, so that the majority of the data came from similar parts of the same CCD module, reducing the importance of instrumental corrections. The corrected *Kepler* eclipse light curves are shown in Fig. 1, with the median out-of-eclipse magnitude ($m_{\text{Kep,med}}$) subtracted. The primary and secondary eclipses have different duration and the phase difference between the eclipses is about 0.6, both of which are indicators of significant eccentricity in the orbits.

2.2. Ground-based Photometry

In order to obtain color information for the binary, we obtained eclipse photometry in BVI_c using the Mount Laguna Observatory (MLO) 1m telescope. The observational details are given in Table 1. Typical exposure times were 300s in B , 180 s in V and 120 s in I_c . The images were processed using standard IRAF⁸ routines to apply overscan corrections from each image, to subtract a master bias frame, and to divide a master flat field frame. A nonstandard aspect of the image processing involved the correction for a nonlinearity in the CCD response that was present as a result of improperly set readout transistor voltages used between December 2008 and November 2013. The following correction (D. Leonard, private communication) $ADU_{\text{cor}} = ADU \cdot [1.01353 - 0.115576 \cdot (ADU/32767) + 0.0296378 \cdot (ADU/32767)^2]$ was applied using the IRAF task *irllincor* to pixel counts on flat field and object images (after overscan and bias subtraction) taken during that time frame. The nonlinearity had small but noticeable effects on photometric scatter and trends within nights of data.

⁸ IRAF is distributed by the National Optical Astronomy Observatory, which is operated by the Association of Universities for Research in Astronomy, Inc., under cooperative agreement with the National Science Foundation.

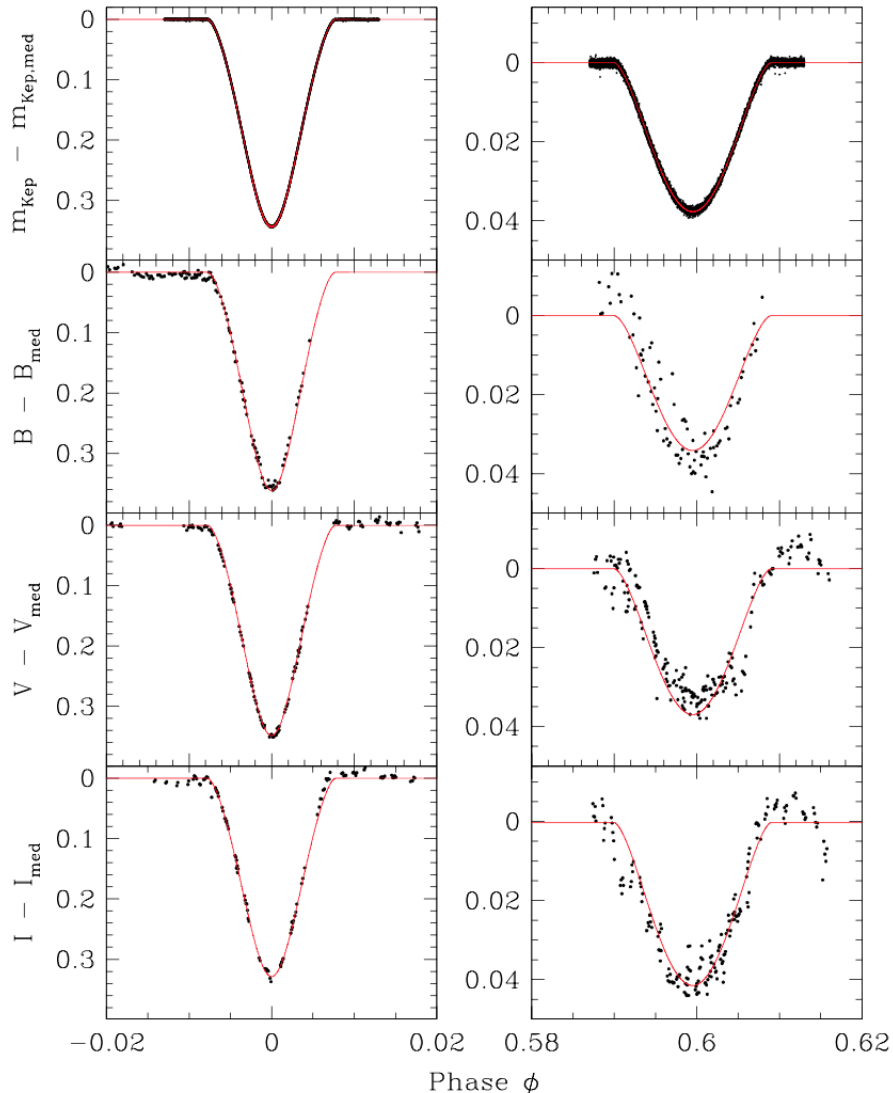


Figure 1. *Top row:* *Kepler* photometry of the primary and secondary eclipse of KIC 9777062. *Bottom rows:* Ground-based BVI_C photometry of the primary and secondary eclipses.

The secondary eclipses of the binary are 0.03 – 0.04 mag deep, and so relatively small data reduction issues can have large effects on the fidelity of the light curve. Our brightness measurements were derived from aperture photometry using DAOPHOT (Stetson 1987), although we took several additional steps to increase the precision of the results. We conducted a curve-of-growth analysis of 12 apertures photometered per star using DAOGROW (Stetson 1990) in order to correct all measured stars to a uniform large aperture. We then attempted to unify the data for each filter to a consistent zeropoint by using ensemble photometry (Sandquist et al. 2003; Honeycutt 1992). This essentially uses all measured stars on the frame to determine magnitude offsets resulting from differences in exposure time, airmass, atmospheric transparency, and the like. Our implementation iteratively fits for position-dependent corrections that result from variations from point-spread function across the frame. These steps each brought noticeable reductions in the amount of scatter in the light curves. However, we still found that the shape of the ground-based light curves of

the secondary eclipse did not match what was expected from the *Kepler* observations. After some investigation, we found that features in the light curve were correlated with those for the brightest star near KIC 9777062 in our images. (The star was about 70 pix or 28'' distant on the sky, so there was no significant overlap of the point-spread function when the seeing was generally 4-8 pix FWHM.) We found that after subtracting the light curve of this star the out-of-eclipse light levels and the shapes of the primary and secondary eclipse light curves were much more consistent from night to night. When more distant stars on the images were tested, we found a much poorer degree of correlation. We conclude that short length-scale variations were not being corrected for (and could not be corrected for, due to lack of star sampling on the image) with whole-image zeropoint corrections or image-scale position-dependent corrections. The variations were of around 0.01 mag size, but could significantly affect the secondary eclipse light curves. We could not identify any features on our flat field images that could explain the light curve variations, and they oc-

curred whether dome flats, twilight flats, or hybrid flats (combining the smoothed large-scale variations from the twilight flats and small-scale variations from dome flats) were used. The ground-based eclipse observations are shown in the bottom rows of Fig. 1.

In addition to the eclipse light curve observations, we took BVI_C images to calibrate photometry to the standard system. In the interest of readability, the discussion of this has been moved to an appendix. In Table 2, we summarize the calibrated out-of-eclipse photometry for the eclipsing binary KIC 9777062 from various sources.

2.3. Spectroscopy of KIC 9777062

Spectroscopic observations were obtained at the Hobby-Eberly Telescope (HET) with the High Resolution Spectrograph (HRS; Tull 1998) as part of normal queue scheduled observing (Shetrone et al. 2007), the Nordic Optical Telescope (NOT) Fibre-fed Echelle Spectrograph (FIES; Telting et al. 2014), and the MMT Hectochelle (Szentgyorgyi et al. 2011).

The configuration of the HET HRS was chosen based upon the spectral line widths and strength of the secondary in the first spectrum taken. KIC 9777062 was observed with the configuration HRS_60k_central_600g5822_2as_2sky_ISO_GC0_2x1 to achieve resolution $R = 60000$. This configuration covers 4825 Å to 6750 Å with a small break at 5800 Å between the red and blue CCDs. Exposure times were 540 or 580 seconds. The data were reduced using the echelle package within IRAF for standard bias and scattered light removal, 1-D spectrum extraction, and wavelength calibration. A nightly correction was made based on observations of radial velocity standard stars, although this was a small correction (typically between 0.2 and 0.4 km s⁻¹).

FIES covers the spectral range 3700 to 7300 Å, and we used the high-resolution mode ($R = 67000$). Each observing epoch consisted of two exposures of 1800 s each. The observations were split to reduce problems with cosmic rays hitting the CCD. The science exposures were preceded by a Th-Ar exposure for accurate wavelength calibration. In daytime before or after each observing night calibration images (7 bias and 21 halogen flats) were obtained. The FIES data were reduced using the FIEStool pipeline⁹, which is a program written in Python to perform bias subtraction, flat fielding, and scattered light subtraction, and using IRAF tasks (via PyRAF) from the echelle package to do spectral order tracing, extraction, and wavelength calibration.

The observations with the Hectochelle multi-object spectrograph covered 5150 to 5300 Å at a resolution of 45000. The science exposures were bracketed by Th-Ar lamp exposures to optimize the wavelength calibration, and preceded by a dome-lamp flat exposure used for tracing the spectra on the CCD.

The radial velocities were derived using a spectral disentangling code written in Python following the algorithm described in González & Levato (2006). In each iteration step the spectrum for each component is isolated by aligning the observed spectra using the measured radial velocities for that component and then av-

eraging. After the first determination of the primary star spectrum, the contribution from one component can be subtracted during the determination of the average spectrum of the other. The radial velocities can also be remeasured using the spectra with one component subtracted. This procedure is repeated for both components and continued until a convergence criterion is met. We use the broadening function formalism (Rucinski 1992) to measure the radial velocities using synthetic spectra from the grid of Coelho et al. (2005) as templates.

The FIES spectra are mostly taken in pairs at 20 different orbital phases sampling the orbit and velocity range well. Both the HRS and the Hectochelle spectra are also well distributed in phase, but with fewer observations. The FIES velocities were calculated as the robust mean measured in 35 spectral orders (the orders 20-55 except order 39 where the wide H β line is). We use these 35 orders out of 79 because the signal-to-noise ratio is too low in the bluest orders and in the reddest orders the spectra are contaminated by telluric lines. For the uncertainty estimates we use the standard error of the mean (standard deviation divided by the square root of the number of measurements) calculated using all 35 orders. Final FIES velocities were recalculated during three iterations of the whole disentangling procedure in which the uncertainties of the primary velocities were used as weights when averaging the component spectra. This is reasonable because we have a large set of spectra with similar signal-to-noise (and hence a small spread in RV uncertainties). We present the velocities with their measurement uncertainties in Table 3. The means of the velocity uncertainties are 168 ± 34 m s⁻¹ and 290 ± 140 m s⁻¹ for the primary and secondary, respectively.

To calculate velocities from the HRS observations, the spectra were split into nine segments and the same procedure was followed with the exception that we did not apply the velocity uncertainties as weights. All were given equal weight with two exceptions given zero weight: one because of very low signal-to-noise and continuum normalization difficulties, and the other because of very low velocity separation between the two components. The means of the uncertainties are 181 ± 84 m s⁻¹ for the primary and 300 ± 110 m s⁻¹ for the secondary.

Although the Hectochelle spectra from the MMT have lower signal-to-noise than the other spectra, we were able to extract radial velocities for both stars at each epoch. Velocities were calculated in the same way as the HRS spectra, but split into seven segments. The uncertainty estimate stated for these measurements is just the rms of the mean value from the sub-sections except in three cases with clear influence of an outlier for which a robust standard deviation was used instead. The means of the uncertainties are 840 ± 150 m s⁻¹ and 1330 ± 315 m s⁻¹ for the primary and secondary, respectively.

The phased radial velocity measurements are plotted in Fig. 2, showing the eccentricity of the orbit. In this situation where we are making use of radial velocities from three different telescopes and instrument configurations, systematic errors can be as important as random ones. We therefore looked at zeropoint offsets between a best fit orbit model and different subsets of data. For measurements from the NOT (both primary and secondary star) and primary star measurements from the HET and

⁹ <http://www.not.iac.es/instruments/fies/fiestool/FIEStool.html>

Table 2
Out-of-Eclipse Photometry for KIC 9777062

Filter	EHK/2MASS	This Paper	G99	J13
U	12.630 ± 0.021		12.711 ± 0.054	12.680 ± 0.006
B	12.616 ± 0.024	12.600 ± 0.002	12.598 ± 0.017	12.575 ± 0.011
V	12.264 ± 0.018	12.241 ± 0.002	12.236 ± 0.001	12.230 ± 0.008
R_C			11.897 ± 0.025	
I_C		11.830 ± 0.003		11.833 ± 0.005
J	11.552 ± 0.022			
H	11.448 ± 0.018			
K_S	11.388 ± 0.018			
V_A		12.74	12.73	12.73
$(B - V)_A$		0.33	0.33	0.33
$(V - I_C)_A$		0.37		0.35
V_B		13.33	13.32	13.32
$(B - V)_B$		0.41	0.41	0.40
$(V - I_C)_B$		0.49		0.47

Note. — EHK: Everett et al. (2012). 2MASS: Skrutskie et al. (2006). G99: Glushkova et al. (1999). J13: Janes et al. (2013).

Table 3
Radial Velocity Measurements

mJD ^a	v_A	σ_A	v_B	σ_B	mJD ^a	v_A	σ_A	v_B	σ_B
		(km s ⁻¹)					(km s ⁻¹)		
NOT FIES Observations									
6080.615695	28.24	0.15	-16.96	0.20	6518.521145	51.66	0.15	-43.50	0.52
6086.702696	-32.85	0.12	52.73	0.17	6518.551091	51.91	0.14	-43.62	0.30
6092.678310	18.32	0.19	-4.24	0.34	6520.484531	72.09	0.14	-66.56	0.28
6093.628552	28.93	0.23	-15.01	0.33	6521.526209	69.33	0.19	-65.40	0.33
6109.611515	-4.47	0.23	23.06	0.42	6521.548053	68.88	0.25	-63.26	1.04
6115.580028	62.44	0.16	-54.49	0.31	6543.464550	-18.18	0.17	35.86	0.21
6115.602482	62.78	0.18	-54.28	0.42	6543.486397	-18.89	0.17	36.34	0.22
6123.583515	-40.60	0.19	61.51	0.28	6549.378082	-25.21	0.15	44.76	0.18
6123.607625	-40.55	0.24	62.07	0.42	6549.399931	-24.95	0.15	44.43	0.21
6227.334731	19.16	0.17	-6.34	0.21	HET HRS Observations				
6389.680638	-19.69	0.17	38.22	0.22	6038.914740	65.17	0.15	-58.16	0.50
6389.702489	-20.05	0.15	38.76	0.23	6039.908239	73.04	0.18	-66.09	0.28
6396.682755	-16.22	0.20	35.42	0.38	6078.813734	72.98	0.15	-67.87	0.29
6396.704618	-16.18	0.15	35.53	0.35	6084.790102	-41.30	0.14	60.92	0.34
6425.623269	64.88	0.20	-57.38	0.32	6109.954081	-1.20	0.16	16.74	0.27
6425.645114	64.44	0.27	-56.79	0.29	6110.719643	7.09	0.24	7.41	0.22
6428.662997	-30.15	0.13	49.82	0.22	6116.719453	72.61	0.19	-64.99	0.29
6428.684842	-30.39	0.13	50.32	0.26	6123.917979	-39.15	0.16	59.74	0.25
6429.666715	-40.33	0.14	62.74	0.33	6125.682043	-29.63	0.15	48.44	0.25
6429.688566	-40.29	0.15	63.09	0.18	6126.683770	-22.70	0.16	39.95	0.21
6430.621638	-41.99	0.15	64.57	0.22	6131.655552	24.09	0.14	-11.02	0.17
6430.643464	-41.91	0.16	64.58	0.25	6133.878550	51.13	0.45	-41.68	0.56
6445.675337	40.42	0.15	-28.68	0.15	MMT Hectoechelle Observations				
6445.697184	39.51	0.14	-27.96	0.16	4401.617194	31.90	0.75	-20.94	0.82
6457.644779	13.90	0.16	-1.35	0.24	5374.659578	-36.13	0.65	56.06	2.03
6457.666628	14.11	0.14	-1.25	0.18	5457.741551	13.62	1.07	2.10	1.43
6489.691312	-37.51	0.17	58.16	0.18	5812.757900	-19.52	1.11	37.18	1.19
6489.711426	-37.64	0.16	57.72	0.24	5812.827731	-21.18	0.87	39.15	1.41
6507.524857	-41.91	0.17	64.16	0.27	6022.842012	31.24	0.79	-18.81	1.29
6507.546702	-41.83	0.17	64.00	0.26	6023.883682	-6.91	0.71	25.53	1.25
6518.448366	50.69	0.13	-42.73	0.31	6024.954796	-31.89	0.77	54.52	1.28

^a mJD = BJD - 2450000.

Hectoechelle, we find mean offsets of less than 0.1 km s⁻¹. For measurements of the secondary star from HET, there was a larger shift of -0.57 km s⁻¹, and +0.52 km s⁻¹ from the Hectoechelle. We opted not to correct for these offsets because the more precise primary star measurements agree better with the NOT data and the model.

3. ANALYSIS OF KIC 9777062

3.1. Cluster Membership

For a cluster like NGC 6811 where the stars are spread over a large area, it is especially important to pay close

attention to cluster membership criteria. Janes et al. (2013) presented photometric and structural data on the cluster. This binary star is projected 13¹/₄ from their cluster center ($\alpha_{2000} = 19^{\text{h}}37^{\text{m}}17^{\text{s}}$, $\delta_{2000} = +46^{\circ}23'18''$), which places it well outside the cluster core, about twice the effective radius determined from exponential or Plummer model fits (Janes et al. 2013). Because it lies in the outskirts of the cluster, it is important to examine other indicators of cluster membership.

The proper motion of KIC 9777062 was measured by Sanders (1971, star 195), Dias et al. (2014), and

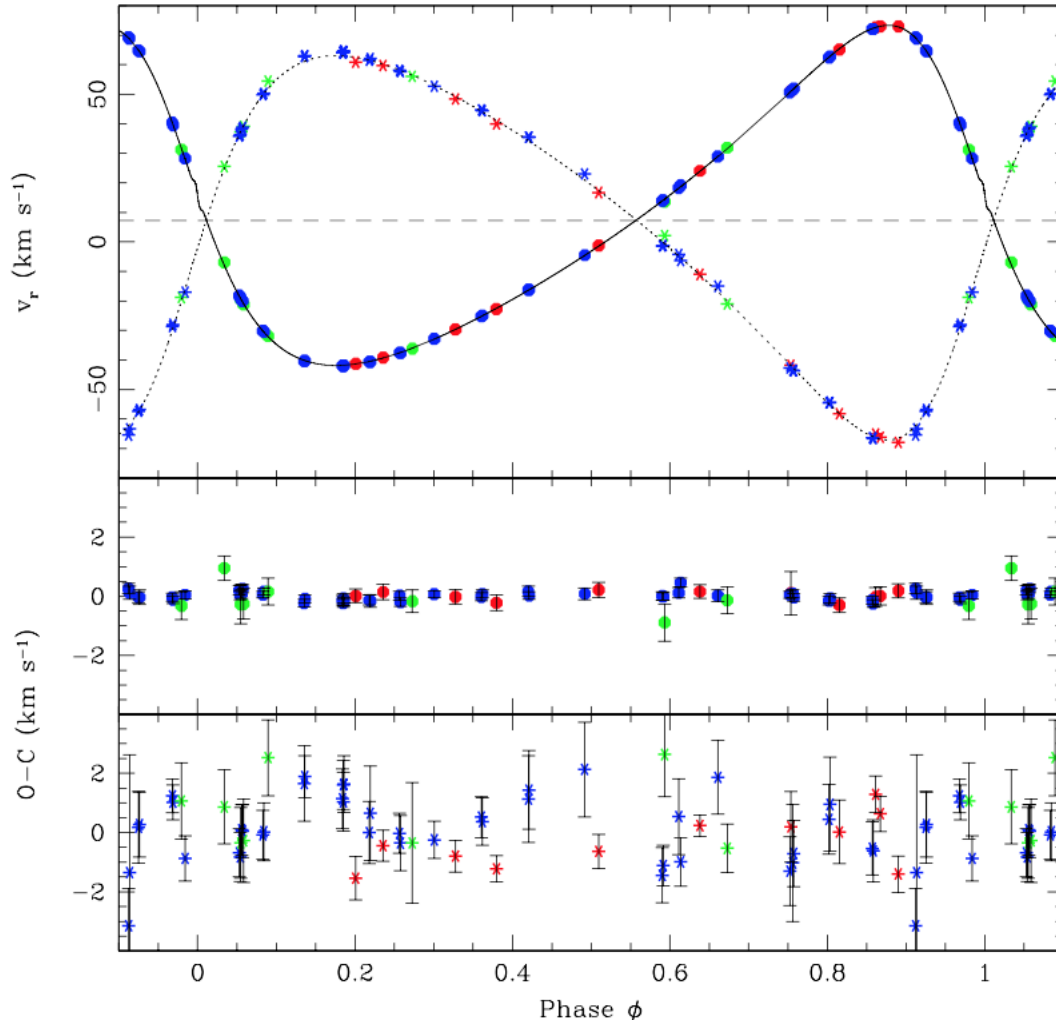


Figure 2. Phased radial velocities for KIC 9777062, along with the best fit model. Observations of the primary star use dots, and secondary star observations use asterisks. Red, blue, and green colors are observations from the HET, NOT, and MMT, respectively. The lower panels show the observed minus computed values with error bars scaled to give a reduced $\chi^2 = 1$ (see §3.4).

Kharchenko et al. (2013), finding membership probabilities of 93%, 96%, and 30%. As for radial velocities, four studies have determined means for the cluster. Frinchaboy & Majewski (2008) spectroscopically identified 7 likely cluster members and determined a mean velocity of $+6.03 \pm 0.30$ km s $^{-1}$ (where the error of the mean is quoted), Mermilliod et al. (2008) found $+7.28 \pm 0.11$ km s $^{-1}$ from three stars, Molenda-Żakowicz et al. (2014) found $+6.68 \pm 0.08$ km s $^{-1}$, and Meibom et al. (2013) find $+7.7 \pm 0.04$ km s $^{-1}$ from hundreds of stars. In addition, 6 giants we identify as likely cluster members have APOGEE radial velocities in Data Release 12 that give a mean value of $+7.70 \pm 0.30$ km s $^{-1}$. KIC 9777062 was actually observed by Frinchaboy & Majewski (2008) (identified as TYC 3556-00370-1), who found a velocity of $+5.92 \pm 1.82$ km s $^{-1}$. Based on the date of their observation (UT 2003 Sept. 16), this was shortly before secondary eclipse (phase $\phi = 0.51$), so their measurement was probably representative of the system velocity of the binary. The system velocities γ for the components of the binary were fitted separately (see §3.4), and

the values ($+7.2$ and $+7.7$ km s $^{-1}$) are fully consistent with the Mermilliod & Mayor and Meibom et al. mean velocities, but less so with the Frinchaboy & Majewski and Molenda-Żakowicz et al. values. One of our HET spectra was also taken quite close to a velocity crossing, and also indicates a velocity of around $+7.2$ km s $^{-1}$. Due to the difficulty of deriving a good cluster mean and velocity dispersion in the face of a large spectroscopic binary population, we regard the binary as a radial velocity member of the cluster. To summarize, the kinematic evidence points to likely cluster membership.

3.2. The Ephemeris And Search for a Third Body

We examined the eclipse timings from the *Kepler* data and ground-based radial velocities in order to look for any evidence of perturbations to the ephemeris due to a third star in a longer orbit about the eclipsing binary or apsidal motion. We used the method of Kwee & van Woerden (1956) to determine the times of mid-eclipse, using short cadence photometry where available to achieve greater timing precision and long cadence photometry in all other cases. The eclipse timings are given in Ta-

Table 4
Kepler Eclipse Timing Observations

mJD ^a	σ (d)	Eclipse Type	Note
4965.58156	0.00012	P	Q1 start
4977.11100	0.00013	S	
4984.81147	0.00029	P	
4996.34134	0.00021	S	
5004.04140	0.00006	P	Q2 start
5023.27175	0.00007	P	
5034.80046	0.00020	S	
5042.50174	0.00010	P	
5054.03076	0.00037	S	
5061.73156	0.00011	P	
5073.26098	0.00013	S	
5080.96170	0.00022	P	
5100.19178	0.00008	P	Q3 start
5111.72165	0.00023	S	
5119.42167	0.00008	P	
5130.94986	0.00049	S	
5138.65199	0.00012	P	
5150.18084	0.00021	S	
5157.88190	0.00011	P	

Note. — A portion of this table is published here to demonstrate its form and content. Machine-readable versions of the full table are available.

^a mJD = BJD - 2450000.

ble 4. All eclipse times were put on barycentric julian date (BJD) barycentric dynamical time (TDB) system, with ground-based times converted from heliocentric to barycentric time using an online tool¹⁰ (Eastman et al. 2010). Based on the higher precision primary eclipse timings, there are no signs of deviations from a linear ephemeris that could indicate the effects of a third body. That best fit ephemeris is

$$(MinI) = 2454965.58156(5) + 19.2300409(11) \times E$$

The timing of secondary eclipses is less precise due to their shallower depths, but the secondary eclipse timings mostly agree with the primary eclipse timings given a phase $\phi = 0.59955$ for the center of the secondary eclipse. There is significant period difference though, which may be evidence of apsidal motion:

$$(MinII) = 2454977.11083(17) + 19.2300245(41) \times E$$

The radial velocity of the binary center of mass provides an additional means of constraining the presence of an orbiting companion. Using the best-fit mass ratio from the binary star models ($q = 0.885$), the center-of-mass velocity can be calculated for each epoch provided the radial velocities of both stars are reliably measured. The results are shown in Fig. 3, but there is as yet no evidence of systematic shifts produced by a tertiary star.

3.3. Spectroscopic Information on the Binary

Spectroscopic constraints on the temperatures and compositions of the binary star components are important to modeling of binary stars (especially for the limb darkening applied to the light curves) and to the translation of the stellar characteristics into distance and age. We analysed the disentangled FIES spectra in order to determine the metallicity and temperature of both stars in the binary.

Spectral disentangling cannot determine the light ratio of unresolved stars, however, so we employed light

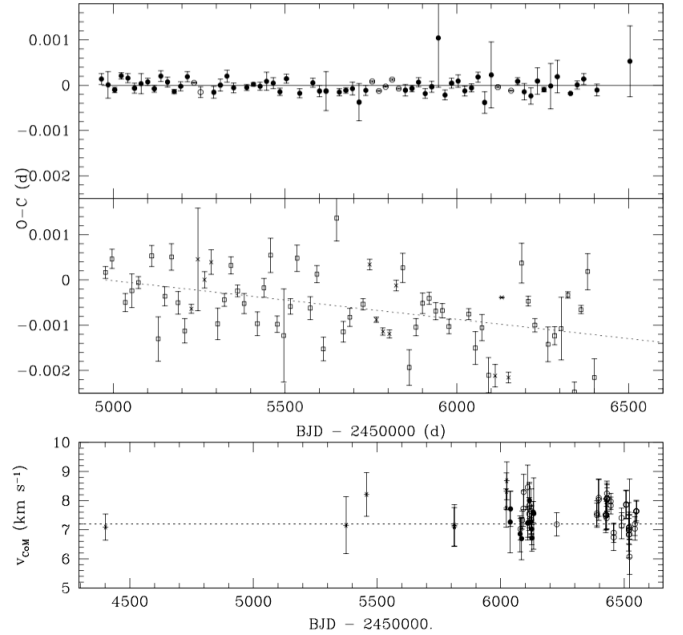


Figure 3. *Top panels:* Observed eclipse times minus computed predictions from the linear best-fit ephemeris for the primary eclipses. Primary eclipses are shown with \bullet (long cadence) and \circ (short cadence), and secondary eclipses are shown with \square (long cadence) and \times (short cadence). *Bottom panel:* Center-of-mass radial velocities for the binary, computed using the best-fit mass ratio $q = 0.885$. HET observations are shown with \bullet , NOT observations are shown with \circ , and MMT observations with $*$, with the fitted system velocity for the primary shown with a dashed line.

ratios in *BVI* filters from the binary analysis (see Table 6) in order to properly gauge line depths. We analysed the spectra of the primary and secondary stars with the preferred value of the light ratios, and for ratios one standard deviation higher and lower. In this way we could estimate the impact of the light ratio on the determined atmospheric temperatures and surface metallicity. Thus, we analysed six spectra in total.

These spectra were analysed using the VWA software package (Bruntt et al. 2010a,b, 2012), and we briefly summarize the analysis here. First, a synthetic spectrum is calculated with preliminary values for T_{eff} , $\log g$, and metallicity. We interpolated the atmospheric model in the MARCS grid (Gustafsson et al. 2008), which uses Grevesse et al. (2007) solar abundances, and atomic data were extracted from the VALD database (Ryabchikova et al. 2015). The computed spectrum was rotationally broadened to fit the width of the observed lines. For the primary we obtained $20 \pm 1 \text{ km s}^{-1}$, and for the secondary, $19 \pm 1 \text{ km s}^{-1}$. This spectrum was compared to the observed spectrum in order to identify approximate continuum windows. In this way we renormalized the output spectrum from the disentangling software using the “rainbow” procedure described in Bruntt et al. (2010a). We note that the renormalization was repeated after improving the atmospheric parameters.

Second, we used VWA to automatically select isolated lines in the spectrum, and each line was fitted to determine the abundance. For each model fit we keep T_{eff} , microturbulent velocity, and metallicity fixed for each run. It is important to note that we did not change $\log g$; instead we used the well-determined values from the binary

¹⁰ <http://astrutils.astronomy.ohio-state.edu/time/hjd2bjd.htm>

Table 5
Spectroscopic Parameters and Abundances for
Eclipsing Binary Components

	Primary	Secondary
$\log g$ (adopted)	4.16	4.22
T_{eff} (K)	7700 ± 150	7150 ± 100
$v_{\text{rot}} \sin i$ (km s $^{-1}$)	20 ± 1	19 ± 1
ξ (km s $^{-1}$)	3.7 ± 0.3	2.0 ± 0.2
[Fe/H]	$+0.46 \pm 0.13$	-0.03 ± 0.13
[Ca/H]	-0.80 ± 0.15	-0.14 ± 0.15
[Ti/H]	-0.10 ± 0.16	-0.03 ± 0.15
[Cr/H]	$+0.35 \pm 0.14$	-0.20 ± 0.15
[Ni/H]	$+0.71 \pm 0.13$	-0.27 ± 0.14

star analysis ($\log g = 4.16$ and 4.22 for the primary and secondary, respectively). After running several models with different T_{eff} and microturbulence, we then used the neutral and singly-ionized iron lines (Fe I and Fe II) to infer the adjustment needed to eliminate any correlation between Fe I abundance and either excitation potential or equivalent width. In addition, we required that Fe II and Fe I lines yield the same mean value for the abundance. In the case of Fe I lines we used a slight adjustment of the abundance due to NLTE effects, following the calculations of Rentzsch-Holm (1996). Interpolating in the figures from Rentzsch-Holm (1996), we added 0.07 dex to the Fe I abundances from VWA.

The atmospheric parameters we determined are given in Table 5, including the uncertainties due to the light ratio and scatter in the Fe I and Fe II abundances. Our analysis found a fairly standard value for the microturbulent velocity ξ for the secondary star (2.0 ± 0.2 km s $^{-1}$), but we found it necessary to use a larger value of 3.7 ± 0.2 km s $^{-1}$ for the primary star. This may be related to possible convective blueshifts in the radial velocities of the primary star, as discussed in §3.4.

The rms scatter in Fe I line abundances was 0.19 for the primary and 0.21 dex for the secondary. This is a relatively high scatter, and likely due to an imperfect disentangling of the spectra. Contributors to the uncertainty on the mean Fe abundance are 0.02 dex due to line-to-line scatter ($\sigma = 0.19/\sqrt{86}$), 0.10 dex due to uncertainties in T_{eff} and microturbulence, and 0.03 due to the light ratio. Furthermore, we adopted a 0.07 dex systematic error from Bruntt et al. (2010b) due to the adopted atmospheric models, NLTE effects, and continuum normalization errors. We add these contributions in quadrature and find the estimated uncertainty on the metallicity to be 0.13 dex for both components. The uncertainty on the elements Ca, Ti, and Cr listed in Table 5 are higher because only 4-8 lines were used. Our Ni abundance is based on 30 lines for the primary and 15 for the secondary.

In Figure 4, we compare the observed spectra of the two stars with synthetic spectra computed using the parameters listed in Table 5. Note that for all elements in the figure’s synthetic spectra, the abundances were scaled with the Fe abundance. The secondary star appears to have an approximately solar Ca to Fe abundance ratio, but the primary star is severely underabundant in Ca relative to Fe. Ni and Cr, on the other hand, are quite overabundant relative to the Sun. Given that other spectroscopic studies of NGC 6811 stars (Molenda-Żakowicz

et al. 2014; Frinchaboy et al. 2013) find abundances close to that of the secondary star, the primary star appears to be anomalous. The signatures of high metal abundances and low Ca abundance identify the primary as a metal-lined Am star. The leading explanation for this phenomenon is diffusion via gravitational settling and radiative levitation (e.g., Turcotte et al. 1998; Richer et al. 2000). Calcium tends to be underabundant because it has a closed electron shell configuration at the temperature of interest, reducing its radiative cross section near the peak wavelengths of the star’s emission. Thus, Ca, unlike Fe and other metallic species, gravitationally settles into deeper layers.

A-type stars are generally rapid rotators, but when they are not, chemical peculiarities are frequently present: Am stars, for example, generally have rotational speeds below 100 km s $^{-1}$ (Abt & Hudson 1971; Niemczura et al. 2015). Both stars in the binary rotate at speeds well below this threshold. That said, both stars are rotating too fast to have pseudo-synchronized to their orbital angular velocities at periastron passage (8.2 and 7.1 km s $^{-1}$; Hut 1981). So tidal effects appear to have forced the rotation rates lower despite the fact that the theoretical predictions for synchronization by dynamical tides (Zahn 1975) give timescales that are several orders of magnitude longer than the ~ 1 Gyr age of the cluster. Carquillat et al. (2004) came to similar conclusions for a sample of field Am stars in binaries. The fact that close to two-thirds of Am stars are members of spectroscopic binaries (Carquillat & Prieur 2007) indicates that tidal effects are an important ingredient in this phenomenon.

For the purposes of our modeling below, this means that the primary star spectrum will not help constrain the bulk (interior) chemical abundances of the stars. We are still left with the measurements of the secondary star and literature measurements of other stars in the cluster, and these are consistent with each other to about 1σ of the secondary star measurement error.

The derived spectroscopic temperatures are 7700 ± 150 K and 7150 ± 100 K for the primary and secondary stars. We computed photometric temperature estimates as checks on these values. Unfortunately, there are fewer well-studied stars for calibrating A and early F stars than there are for G, K, and M spectral types. We employed relations given by Casagrande et al. (2010) and Boyajian et al. (2013), although it should be noted that there are roughly twice as many A star calibrators in the Boyajian et al. paper and thus their value should be considered to be better constrained. We used the system photometry, luminosity ratios derived from the binary modeling, metallicity [Fe/H] = $+0.04$, and an average reddening $E(B - V) = 0.07 \pm 0.02$ (see §1.1) in empirical relations using optical colors.

Using Casagrande et al. (2010) relations, we used the $(B - V)$ color to calculate the primary star (7330 K) and secondary star (6950 K) temperatures. These are $1 - 2\sigma$ smaller than the spectroscopic values for both stars, but the stars are at the blue end of the quoted range of reliability for the color-temperature relations. [The $(V - I_C)$ color could not be used because the stars were outside the color range.] Using Boyajian et al. (2013) relations, temperatures from $(V - I_C)$ colors (around 7590 and 6990 K for the primary and secondary stars, respectively) are

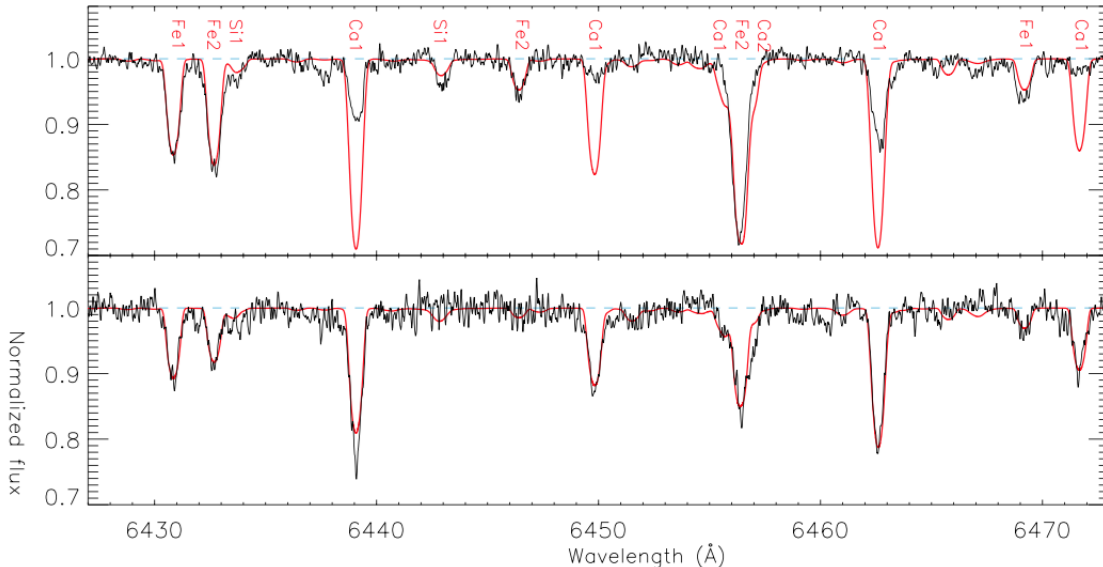


Figure 4. Comparison of disentangled spectra for the KIC 9777062 primary (*top panel*) and secondary (*bottom panel*) with best-fit synthetic spectra (*red lines*) in the vicinity of four Ca I lines.

consistent with the spectroscopic values, but the six parameter ($B - V$) color relation produces much lower values (7040 and 6690 K, respectively). There are, however, few calibrators in the vicinity of the color of our stars, and the fit may be going too low. In addition, the uncertainty due to the reddening is approximately 100 K using $B - V$ colors.

The Am phenomenon operating in the primary star is known to produce line blanketing in the blue part of the spectrum, and this makes an Am star redder than it would otherwise have been. Using the $(B - V) - T_{\text{eff}}$ calibration specifically for Am stars from Netopil et al. (2008), we derive $T_{\text{eff}} = 7620 \pm 175$ K for the primary star, in excellent agreement with the spectroscopic temperature.

There are benefits in also comparing the spectroscopic temperatures with stars very similar to the ones in KIC 9777062 in well-studied eclipsing binary systems: single stars in this range of spectral types tend to be rapidly rotating, which can produce significant gravity darkening and effects due to the angle of observation. An excellent comparison is XY Cet B (Southworth et al. 2011). This star has nearly identical mass (0.2% difference) and similar radius (1.5% difference, with XY Cet B larger) as KIC 9777062 A, and both are Am stars. Southworth et al. found that the characteristics of XY Cet agree best with isochrones for a solar bulk composition and age slightly less (850 Myr) than NGC 6811. But because both stars in XY Cet are Am stars, the bulk composition cannot be directly determined, which could impact the temperatures and the age determination. Otherwise, these indicators point to unusually good agreement between XY Cet B and KIC 9777062 A. Southworth et al. adopt a temperature of 7620 ± 125 K based on comparisons with synthetic spectra and Strömgren photometry, in good agreement with our spectroscopic temperatures.

KIC 9777062 B is similar (less than 2% difference in mass and radius) to HY Vir B, with HY Vir B the lower

mass star (Sandberg Lacy & Fekel 2011). The HY Vir system appears to be similar in age to NGC 6811, but probably slightly older (1.35 Gyr). Although the chemical composition for HY Vir has not been spectroscopically measured, the authors find that a super-solar metallicity fits the masses and radii of the stars in the binary. Lower mass, higher age, and higher metallicity would all push the star in the direction of lower temperature, so their quoted value for HY Vir B (6550 ± 120 K) should be considered a lower limit for KIC 9777062 B. On the other hand, V501 Mon B (Torres et al. 2015) is approximately 2% larger in mass and has a very similar age (1.1 Gyr) and composition ($[\text{Fe}/\text{H}] = +0.01$). Its temperature (7000 ± 90 K) is roughly consistent with that of KIC 9777062 B.

In conclusion, we are choosing to depend on the spectroscopically derived temperatures in our analysis below. This decision is partly based on the difficulties in using photometry to determine temperatures for A stars: there are currently small numbers of calibrators for A stars, disagreement between color-temperature relations from different researchers, and questions of how applicable single star calibrations can be for slowly rotating stars (as in our eclipsing binary). However, the photometric temperature for the primary from an Am star calibration does support our spectroscopic value.

3.4. Binary Star Modeling

To simultaneously model the ground-based radial velocities and photometry and *Kepler* photometry, we used the ELC code (Orosz & Hauschildt 2000). We fitted the binary with a primary set of 14 parameters: orbital period P , reference time of conjunction (primary eclipse) t_c , velocity semi-amplitude of the primary star K_1 , mass ratio $q = M_2/M_1 = K_1/K_2$, systematic velocities for both stars γ_1 and γ_2 , eccentricity e , phase difference between eclipses $\Delta\phi$, inclination i , ratio of the primary radius to average orbital separation R_1/a , ratio of radii R_1/R_2 , temperature ratio T_2/T_1 , and contamination of

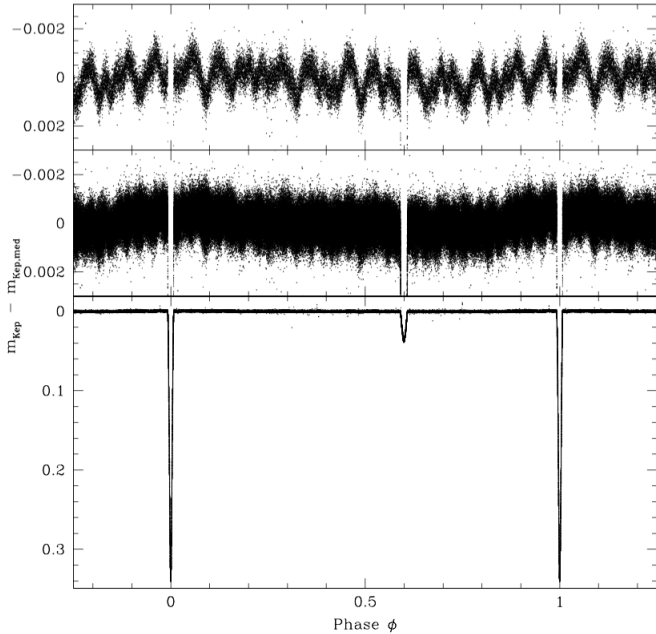


Figure 5. Short cadence *Kepler* data versus orbital phase. *Top panel:* One orbit cycle from quarter 10, showing pulsations. *Middle panel:* All data, zoomed on the out-of-eclipse variations, showing the reflection effect. *Bottom panel:* All data, showing the positions and depths of eclipses.

the *Kepler* light curve in the two seasons of short cadence observations. The *Kepler* contamination parameters are used to account for possible dilution of the light curves by stars that are not physically associated with the binary. *Kepler* pixels and stellar point-spread functions are large by the standards of most ground-based cameras, and it is more difficult to disentangle the light of blended stars. The contamination parameters did not play a major role in the fits, however, because there are no bright contaminating stars nearby. In the fits, the contamination parameters themselves are found to be quite small (0.03% and 0.45% for the two seasons), in accord with values from the *Kepler* Input Catalog (see §2.1).

The light curve is quite flat outside of eclipses, with a small reflection effect (full amplitude about 0.001 mag) observable in the *Kepler* data (see Fig. 5). The maximum occurs around primary eclipse, with a minimum centered on the secondary eclipse. The variation is asymmetric, in accord with the eccentricity of the orbit. While this type of variation can provide critical information for binaries that do not eclipse (Faigler & Mazeh 2011), its physical content is outweighed by the eclipse observations, and we removed the small reflection effect from our light curves and restricted our modeling to eclipses and phases shortly before and after them.

Gravity darkening should have a negligible effect on the light curves due to the slowly rotating, nearly spherical stars in this fairly wide binary. However, limb darkening plays an important role in the determination of the system parameters because only the limb of the secondary star is eclipsed, thanks to the eccentricity of the orbit and its orientation with respect to the line of sight. In turn, the shallowness of the secondary eclipse results in a relatively low signal-to-noise ratio in measurements. As a result, we find that we are unable to reliably fit for the

coefficients of a limb darkening law in any passband except *Kepler*'s. The most important effect of this is on the determination of the luminosity ratios that are needed to constrain the color-magnitude positions of the two stars (§4.2.2).

To assess the possible systematic errors, we approached the limb darkening in several ways. A common problem in light curve fitting is that the coefficients of the limb darkening laws are correlated, and fits can sometimes even leave the regime of realistic values. If theoretical values are used, systematic errors in T_{eff} , $\log g$, or composition will lead to systematic errors in fitted parameters. Given the chemical peculiarities seen for the primary star, it is reasonable to wonder whether we could rely on any theoretical coefficients even if T_{eff} and $\log g$ were perfectly known. In our first approach (inspired by Brogaard et al. 2011), we used a quadratic limb darkening law for each passband, held the BVI_C coefficients fixed at values determined from ATLAS atmospheres (Claret 2000) for the estimated effective temperature and gravity of the star, and fitted for one parameter for each star in the *Kepler* passband. Even if our fixed *Kepler* coefficients are in error, this should be largely compensated for by a change in the other (correlated) parameter. In the second approach, we again used a quadratic law, but used the algorithm of Kipping (2013) to fit for both coefficients for both stars in the *Kepler* passband. Kipping recasted the limb-darkening coefficients in a way that reduces correlation, and which allows for straightforward sampling of the triangular region of physically realistic values. This last point means that our ignorance about the precise form of the limb darkening for the stars can be fully accounted for in the uncertainties of the derived parameters of the binary system. Kipping's method has been implemented in the ELC code. In the third method, PHOENIX atmosphere models (Hauschildt et al. 1997) were used to calculate the relative contributions from the two stars to the total flux, but the limb darkening coefficients were fitted using the Mandel & Agol (2002) algorithm. This approach is somewhat inconsistent in that the limb darkening in the atmosphere models will not be the same as used in fitting the light curve. However, the relationship between the fitting parameters and the relative contributions to the total system luminosity will be based on a more sophisticated description of the stellar atmospheres.

We applied the spectroscopic temperature of the primary star T_1 (see §3.3) as an observed constraint, allowing the value to vary, but applying a χ^2 penalty if the value deviated from the input. From numerical experiments, we found that the models were generally pushed toward temperatures at the high end of the range (7800 – 7900 K) by the combination of *Kepler* photometry and ground-based observations of the primary eclipse in at least one filter band, despite the χ^2 penalty. The depth of the ground-based primary eclipse observations helps set the temperature in combination with the temperature ratio information from the relative sizes of the primary and secondary eclipses derived from the precise *Kepler* observations. These shifts are within about 1σ of the spectroscopic temperature, however.

The quality of the model fit was quantified by an overall χ^2 , and the minimum value was sought first using

a genetic algorithm (Metcalf 1999; Charbonneau 1995; Orosz et al. 2002) to explore a large swath of parameter space, followed by Markov chain Monte Carlo modeling (Tegmark et al. 2004) to explore models near the minimum and to estimate the uncertainties in the binary model parameters. The quoted parameter uncertainties are based on the range of values that produce a total χ^2 within 1 of the minimum value, which approximates a 1σ uncertainty (Avni 1976). The same procedure was used to determine uncertainties in the masses and radii of both stars.

Because the uncertainties for the measurements are used in the calculation of χ^2 , it is important that these uncertainties are as realistic as possible. We therefore scaled the uncertainty estimates for the radial velocity and photometric observations in order to return a reduced χ^2 value of 1 for each type of measurement. (For example, the reduced χ^2 value for *Kepler* photometry was used to scale the *Kepler* photometry uncertainties, the reduced χ^2 value for the NOT radial velocities of the primary star was used to scale those uncertainties, and so on.) This procedure forces the measurement uncertainties to be consistent with the observed scatter around a preliminary best fit model. After this scaling (by the square root of the reduced χ^2), we computed final models to determine the binary model parameters and uncertainties.

For the different photometric datasets the scaling factors were similar: from 1.30 for *B* up to 1.49 for *Kepler*. This procedure was especially important for the velocities because the scatter of the secondary radial velocities around best fit models was always found to be considerably higher than implied by the measurement uncertainties. For the NOT velocities, we needed to scale by a factor of 3.8, and for the HET data, by a factor of 2.1. (For comparison, we found that the rms variation in the primary star velocities was almost exactly what was expected from the intrinsic measurement uncertainties according to a χ^2 test, and the scaling factors were less than 10%.) So, there appears to be a source of velocity variability intrinsic to the secondary star producing this. The variability may be related to the pulsation of the secondary star (see §4.1.2), but we did not find a correlation between the velocity residuals and the pulsations in the *Kepler* light curve. From test models, we find that the best fit orbit can be pulled from the better determined solution implied by the primary star. That said, we do not want to discount the secondary star velocities (and indeed, we cannot if we want to determine masses for the component stars). To address this, we independently fitted an orbit to the secondary star velocities and used the scatter around this solution to scale the velocity uncertainties (and effectively, the weights) we used in our final combined fit. This way the secondary star velocities contribute to determination of parameters like the eccentricity e and the argument of periastron ω , but we acknowledge that there are non-orbital effects on them. The reader should be aware that the differences in weighting the velocities decreased the final masses of about 0.016 and $0.008M_\odot$ for the two stars relative to weights based on scatter around the combined fit. Because this shift is larger than the statistical uncertainties in the model fits, we quote these systematic uncertainties

along with our best fit masses. We also include a systematic contribution to the uncertainty due to the possible shift in secondary eclipse phase with time (Figure 3): by not modeling this shift we may be introducing scatter in the *Kepler* eclipse light curves that would appear as a small increase in the derived eclipse widths and radii. Based on the potential shifts, we estimate this effect to come to about $0.002R_\odot$ for both stars.

Figures 1 and 2 show comparisons of the *Kepler* light curves and radial velocities with the best fit model, and Table 6 shows the parameters of the best fits. For the runs using Kipping’s algorithm for the limb darkening, we identified three local minima with χ^2 within 1 of the minimum value found. These minima appear to have involved values of the primary star limb darkening coefficients and other parameters (like inclination) that depend on the limb darkening. When reporting the best fit values in the table, we give one-sided error bars when the two higher local minima were both on the same side of the apparent global minimum. The systematic differences between the results using different limb darkening algorithms are one indicator of our limits in being able to reduce parameter uncertainties. For our adopted parameters, we use a weighted mean of the values from the three methods with a quoted uncertainty from a quadratic summation of the fit uncertainties (from the χ^2 analysis) and the scatter in the values from the three methods.

As described earlier, the decomposition of the system photometry into the contributions from the individual stars cannot be done particularly precisely using eclipse depths. We have derived our final luminosity ratios from a straight mean of the results for the three limb darkening algorithms, using the dispersion in the results as a measure of the systematic uncertainty. We find $L_2/L_1(B) = 0.540 \pm 0.006$, $L_2/L_1(V) = 0.581 \pm 0.005$, and $L_2/L_1(I_C) = 0.6492 \pm 0.0008$.

One of the interesting results of our modeling is the persistent difference between the system velocities γ_1 and γ_2 derived for the two stars, with the primary having a velocity that is lower by about $0.45 - 0.55 \text{ km s}^{-1}$. A difference of approximately this size is present when the velocities from each of the telescopes are modeled separately, which appears to rule out velocity zeropoint issues although denser radial velocity sampling of the orbit is needed to be definitive. Differences like this can potentially be induced by gravitational redshifts or convective blueshifts if the properties of the stars are different enough. Using the binary star analysis, the difference in gravitational redshifts is only expected to produce a difference of about 2 m s^{-1} , which can be neglected here. Convective blueshifts result from asymmetries in the motions of gas near the surface: outward moving parcels are generally hotter, brighter, and cover a larger fraction of the surface than inward moving parcels. These motions distort line profiles, but also shift line centers. Convective blueshifts for the Sun reach 300 m s^{-1} (Dravins 1999), and may reach 1000 m s^{-1} for mid-F stars according to models (Dravins & Nordlund 1990) and spectroscopic observations (Allende Prieto et al. 2002). The microturbulence velocity parameter ξ (an indication of the local velocity dispersion in the stellar photosphere) also corroborates the idea that convection is not only hap-

Table 6
Best-Fit Model Parameters for KIC 9777062

Parameter	Quadratic Law	Kipping Algorithm	Atmospheres/MA02	Adopted
T_1 (K)		7700 ± 250 (constraint)		
$x_{Kep,1}$	0.2210 (fixed)			
$y_{Kep,1}$	0.4193 ^{+0.0043} _{-0.0011}			
$x_{Kep,2}$	0.2767 (fixed)			
$y_{Kep,2}$	0.3587 ^{+0.0023} _{-0.0050}			
$x_{B,1}$	0.3603 (fixed)		0.5259 (fixed)	
$y_{B,1}$	0.3671 (fixed)		0.2484 (fixed)	
$x_{B,2}$	0.4033 (fixed)		0.5369 (fixed)	
$y_{B,2}$	0.3294 (fixed)		0.2752 (fixed)	
$x_{V,1}$	0.2763 (fixed)		0.3944 (fixed)	
$y_{V,1}$	0.3535 (fixed)		0.2226 (fixed)	
$x_{V,2}$	0.2979 (fixed)		0.4037 (fixed)	
$y_{V,2}$	0.3375 (fixed)		0.2344 (fixed)	
$x_{I,1}$	0.1270 (fixed)		0.2032 (fixed)	
$y_{I,1}$	0.3262 (fixed)		0.1429 (fixed)	
$x_{I,2}$	0.1493 (fixed)		0.2254 (fixed)	
$y_{I,2}$	0.3255 (fixed)		0.1572 (fixed)	
P (d)	19.2300391	19.2300390	19.2300392	19.2300391
σ_P (d)	0.0000002	0.0000003	+0.0000002 -0.0000004	0.0000003
$t_C - 2450000$	5234.802024	5234.802025	5234.80202	5234.802025
σ_t	0.000007	0.000010	0.00001	0.000011
γ_1 (km s ⁻¹)	7.203 ± 0.002	7.193 ± 0.002	7.193 ± 0.002	7.196 ± 0.005
γ_2 (km s ⁻¹)	7.660 ± 0.004	7.655 ± 0.004	7.657 ± 0.005	7.657 ± 0.005
q	0.885 ± 0.002	0.885 ± 0.002	0.885 ± 0.002	0.885 ± 0.002
K_1 (km s ⁻¹)	57.58 ± 0.03	57.58 ± 0.03	57.58 ± 0.02	57.58 ± 0.03
K_2 (km s ⁻¹)	65.06 ± 0.12	65.05 ± 0.12	65.05 ± 0.13	65.05 ± 0.13
i (°)	87.2517 ± 0.0005	87.2592 ± 0.0009	87.255 ± 0.001	87.254 ± 0.004
e	0.3530 ± 0.0001	0.3517 ± 0.0002	0.3517 ± 0.0002	0.3526 ± 0.0007
ω (°)	65.13 ± 0.01	65.02 ± 0.01	65.02 ± 0.02	65.07 ± 0.05
$\Delta\phi$	0.599340	0.599341	0.599342	0.599341
$\sigma_{\Delta\phi}$	0.000002	0.000002	0.000003	0.000003
R_1/a	0.04007 ^{+0.00002}	0.03987 _{-0.00001}	0.03990 ± 0.00001	0.03991 ± 0.00010
R_2/a	0.03543 _{-0.00002}	0.03534 ^{+0.00002}	0.03531 ± 0.00002	0.03536 ± 0.00006
R_1/R_2	1.1311 ± 0.0008	1.1281 ± 0.0008	1.1301 ± 0.0002	1.1300 ± 0.0015
$(R_1 + R_2)/a$	0.07550 ± 0.00002	0.07522 _{-0.00003}	0.07521 ± 0.00002	0.07533 ± 0.00015
T_2/T_1	0.9237 ± 0.0005	0.9223 ± 0.0003	0.9233 ± 0.0003	0.9229 ± 0.0007
contam. (S0)	0.00453	0.00424	0.00439	
contam. (S2)	0.00028	0.0	0.00015	
$L_2/L_1(B)$	0.5445 ± 0.0012	0.5431 ^{+0.0006} _{-0.0014}	0.5336 ± 0.0015	0.540 ± 0.006
$L_2/L_1(V)$	0.5834 ± 0.0012	0.5831 ^{+0.0006} _{-0.0012}	0.5752 ± 0.0014	0.581 ± 0.005
$L_2/L_1(I_C)$	0.6493 ± 0.0013	0.6499 ^{+0.0007} _{-0.0011}	0.6483 ± 0.0012	0.6492 ± 0.0008
M_1/M_\odot	1.602 ± 0.007	1.604 ± 0.006	1.604 ± 0.007	1.603 ± 0.006 ± 0.016
M_2/M_\odot	1.418 ± 0.003	1.420 ± 0.003	1.420 ± 0.003	1.419 ± 0.003 ± 0.008
R_1/R_\odot	1.749 ± 0.002	1.741 ± 0.002	1.742 ± 0.002	1.744 ± 0.004 ± 0.002
R_2/R_\odot	1.546 ± 0.002	1.543 ± 0.002	1.542 ± 0.002	1.544 ± 0.002 ± 0.002
$\log g_1$ (cgs)	4.157 ± 0.002	4.161 ± 0.002	4.161 ± 0.001	4.160 ± 0.003
$\log g_2$ (cgs)	4.211 ± 0.001	4.213 ± 0.002	4.214 ± 0.001	4.213 ± 0.002

pening in the outermost layers of A stars, but is more vigorous in Am stars than in cooler stars (Landstreet 1998; Landstreet et al. 2009; Gebran et al. 2014). In fact ξ appears to rise from around 2 km s⁻¹ between 6000 and 7000 K up to a maximum of about 4 km s⁻¹ at $T_{\text{eff}} \sim 8000$ K before decreasing to zero at about 10000 K. Spectral synthesis of KIC 9777062 supports this: the spectra appear to require ξ of 3.7 and 2.0 km s⁻¹ for the primary and secondary stars. Because the secondary star is a pulsator, there is a possibility that the pulsation might somehow be causing the difference in γ . Based on the nature of the pulsations (see the top panel of Figure 5), we do not see clear evidence that it is could be due to a higher probability of taking spectra at light curve minima. However, denser coverage of the radial velocity curve should be undertaken to rule out the pulsation.

These behaviors indicate that the KIC 9777062 binary may show something close to the maximum contrast in

convective blueshifts between two stars. The magnitude of the blueshift difference between the two stars can reasonably be expected to be on the order of a few hundred m s⁻¹, and it appears to be working in the theoretically-expected direction. Modeling this is beyond the scope of this work, but this system demonstrates that well-studied eclipsing binaries containing Am stars could contribute significantly to the understanding of the atmospheres of these stars. We have examined the literature on other eclipsing Am stars, but have not found as clear a case as this. V501 Mon (Torres et al. 2015) is a system with parameters similar to KIC 9777062, and would be a good candidate to further study this effect.

4. DISCUSSION

One of the important uncertainties in the discussion below about the eclipsing binary specifically and the cluster generally is the metallicity of cluster stars. Previous spectroscopic measurements were summarized in

§1.1. For the purposes of comparisons with theoretical models from different sources, we will use heavy element mass fraction Z . This is close to an absolute abundance indicator, and will therefore minimize systematic differences between isochrones due to chemical composition. $[\text{Fe}/\text{H}]$ and $[\text{M}/\text{H}]$ are relative indicators of heavy element abundance, of course, and because the assumed solar abundance values are not the same from isochrone set to set, there will be systematic differences between models for the same value of $[\text{Fe}/\text{H}]$. There remain unresolved issues in determining the total solar photospheric heavy element fraction, and this will be a significant uncertainty in our modeling below. Values range from $Z_{\odot} = 0.0122$ (Asplund et al. 2005) to more recent ones like $Z_{\odot} = 0.0153$ (Caffau et al. 2011).

The APOGEE results for NGC 6811 red clump stars imply $Z \approx 0.0137$ (from the combination of the measured $[\text{M}/\text{H}]$ and assumed $Z_{\odot} = 0.0122$), and this will be our preferred choice for use in isochrones. However, because of the lingering disagreements between solar abundance tabulations, we will examine $Z \approx 0.017$ as a possible alternate composition for NGC 6811 stars.

4.1. The Color-Magnitude Diagram

To make the most effective use of the information in the CMD, we have vetted cluster members using proper motions and radial velocities from the literature where possible. We have attempted to use a uniform set of photometry covering as much of the field as possible, using the Janes et al. (2013) dataset supplemented for a few stars with Glushkova et al. (1999) photometry as well as our own. (The comparisons in §2.2 show that these datasets are have the same photometric zero-points to within 0.02 mag.) We will primarily focus on the turnoff region ($V \lesssim 13.8$) for which proper motion membership probabilities are available from Sanders (1971) or Kharchenko et al. (2013)¹¹, or have been calculated by Dias et al. (2014) or can be calculated from the Fourth US Naval Observatory CCD Astrograph Catalog (Zacharias et al. 2013, UCAC4). Because of occasional large disagreements between studies, we do not eliminate any stars from consideration if they have proper motion membership probabilities $P_{\mu} > 50\%$ in any of the studies.

Radial velocities in the field have been published for stars in the vicinity of the giant branch (10 stars, Mermilliod & Mayor 1990; 60 stars, Glushkova et al. 1999) and for stars near the giant branch and upper main sequence (64 stars, Frinchaboy & Majewski 2008; 15 stars, Molenda-Żakowicz et al. 2014). Radial velocity membership measurements by S. Meibom for 5 red clump stars were presented by Stello et al. (2011b), and the APOGEE project (Wilson et al. 2010; Alam et al. 2015) has also released spectroscopic observations for 2 AGB and 4 red clump stars we identify below. In general, there are only a handful of observations per star from these sources. S. Meibom has an extensive database of unpublished radial velocity measurements that we use here in a limited fash-

¹¹ We only use the “kinematic” or proper motion membership probabilities from this study, and not the probabilities based on spatial position or photometry. It should also be noted that Kharchenko et al. (2013) membership probabilities were calculated in a different way than Sanders (1971), who accounted for the distribution of non-members in the field. Thus, the probabilities are not precisely comparable.

ion. We report the radial velocity membership as “Y” if there is no significant variation in all of the measurements or if an orbital solution allows us to identify that the system velocity is consistent with the cluster mean ($\sim 7 \text{ km s}^{-1}$). If there was significant radial velocity variation, but the system could potentially be a cluster member, we identify the star with a “B” (for binary candidate). If there is little or no chance that the system is a member of the cluster, we identify it with an “N”. Without an even more extensive velocity survey of the cluster that can reliably determine systematic velocities of multiple star systems, the velocities will not give a definitive determination of cluster membership, and we will be limited in our ability to use them to identify where the single star locus should be in the CMD. For the stars with $V < 12$, both radial velocity and proper motion membership information is usually available.

Sky position can also be used as circumstantial evidence of membership — the cluster stellar density profile becomes so small beyond about two effective radii that the default should be that these are not cluster members. However, it is reasonable to expect that there are a small number of stars in the cluster outskirts, and we do indeed find stars where all other indicators are for membership. In Tables 8 – 10, we give a simple position membership indication (“Y” or “N”) based on whether each star lies within or without $13'$ from the cluster center.

Below is a short discussion of the stars in some important groups.

4.1.1. Red Clump Stars and Asteroseismology

Masses derived from eclipsing binaries can benchmark masses inferred from asteroseismology. For star clusters in the *Kepler* field, the asteroseismic targets with detectable solar-like oscillations are on the giant branch and in the red clump, while eclipsing binaries have only been found on the subgiant branch and fainter. However, when used in concert with theoretical models, the eclipsing binaries do make it possible to predict giant star masses. In the asteroseismology arena, there is still need to validate masses against accurate and precise measurements. In the so-called direct method, which is likely to have the widest application in astronomy in the near future, masses are derived from scaling relations using the observables $\Delta\nu$ (the frequency separation of overtone modes) and ν_{max} (the frequency of maximum power) along with T_{eff} . For the two older open clusters in the *Kepler* field, preliminary comparisons have been made between asteroseismic masses and predictions from theoretical models anchored with eclipsing binary measurements. In both the ~ 8 Gyr cluster NGC 6791 (Brogaard et al. 2012) and the ~ 2.5 Gyr cluster NGC 6819 (Sandquist et al. 2013), predicted red giant masses are lower than calculated from asteroseismic scaling relations. However, there is strong evidence that the offset between binary-star and asteroseismic-inferred masses is reduced significantly when stellar model-informed corrections are applied to $\Delta\nu$ in the seismic scaling relations (Brogaard et al. 2016, 2015; Sharma et al. 2016). An examination of NGC 6811’s red clump stars allows us to extend the comparison to more massive stars. The clump stars in NGC 6811 did not undergo a degenerate flash at helium fusion ignition — this starts to happen in star clusters with ages near 1.5 Gyr (Girardi et al. 2000,

2009). Thus we will be probing the so-called secondary red clump (hereafter RC2) stars that have a different evolutionary history.

We therefore re-examined stars in the cluster field with photometry putting them in the vicinity of the red clump. Most of these have been discussed by Stello et al. (2011b), Janes et al. (2013), and Molenda-Żakowicz et al. (2014), and their vital data is summarized in Table 8. According to proper motion measurements, four candidates are unanimously cluster members, while the remaining four have membership probabilities less than 50% according to one or two studies (most often Kharchenko et al. 2013), while the others indicate high likelihood of membership. Available radial velocity information indicated membership for all of the candidates with the exception of KIC 9655101 in Frinchaboy & Majewski (2008), which may be a single-lined spectroscopic binary (Molenda-Żakowicz et al. 2014). KIC 9655167 is also identified as a single-lined spectroscopic binary by Molenda-Żakowicz et al. (2014) and Mermilliod & Mayor (1990), and shows radial velocity variability in the survey by S. Meibom. Glushkova et al. (1999) identify KIC 9532903 as velocity variable although Molenda-Żakowicz et al. (2014) do not see variability in their two measurements.

In addition to providing a way of estimating the stellar masses and radii, asteroseismic measurements can be used to examine cluster membership of individual stars, as shown by Stello et al. (2011b). This involves exploiting the correlation between the asteroseismic observables and apparent magnitude for stars with very similar mass and effective temperature. The asteroseismology of seven stars (one early AGB and six red clump) have been discussed by different authors (Stello et al. 2011a,b; Hekker et al. 2011; Corsaro et al. 2012), but we have redone the asteroseismic analysis of the nine NGC 6811 candidates using all available long-cadence data from *Kepler* (starting with either quarters 0 or 1 and reaching quarter 17) in Data Release 23. The longer time baseline compared to previous studies has allowed us to reduce the previously determined uncertainties on the asteroseismic parameters $\Delta\nu$ and ν_{\max} by almost a factor of 1.5 – 2 relative to Corsaro et al. (2012). The sample of stars and the precision of the asteroseismic observables will therefore be about the best currently possible for this cluster.

PDC pipeline data in contiguous sections were fit with a low-order polynomial in order to remove instrumental trends and quarter-to-quarter zero-point differences. The time series were analyzed using the pipeline method of Huber et al. (2009), which provided the values of $\Delta\nu$ and ν_{\max} including uncertainties derived following Huber et al. (2011). The observables are presented in Table 8.

One candidate (KIC 9897838) had no detectable oscillations, and along with its bluer color, we believe it is likely to be a field star. The rest of the candidates show a tight correlation between $\Delta\nu$ and either K or V magnitude with the possible exception of KIC 9409513 (see Fig. 6). We also compared predicted and observed values of $\Delta\nu$ and ν_{\max} in the same manner as Stello et al. (2011b). Those authors employed scaling relations cast using powers of mass, effective temperature, and luminosity to predict the asteroseismic observables from stellar photometry assuming a common mass for the gi-

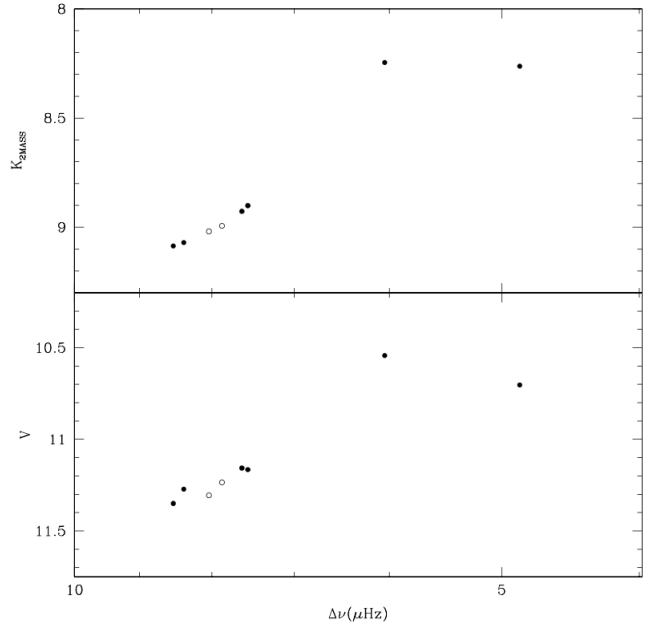


Figure 6. Apparent magnitude versus asteroseismic large frequency spacing $\Delta\nu$ for giant star candidates in NGC 6811. Single-lined spectroscopic binaries are shown with open symbols.

ants, and a distance modulus and reddening for the cluster. This method indicates that all of the remaining red clump stars are highly probable cluster members, while the two potential AGB stars deviate more from the predicted values. The brighter one (KIC 9409513) deviates the most, but its photometry could possibly be explained by a blend with a bright main sequence star. The star is classified as a radial velocity member, but some individual APOGEE elemental abundances deviate mildly ($\sim 0.10 - 0.15$ dex) from those of other clump stars. The asteroseismic scaling relations imply that KIC 9409513 is larger than the cluster clump stars ($8 - 9R_{\odot}$), consistent with having evolved past its core helium burning phase. This conclusion is insensitive to error in T_{eff} resulting from a stellar blend that affects the color.

Based on the weight of the evidence (including CMD position), KIC 9716522 is an unambiguous AGB star cluster member, KIC 9409513 is a possible additional cluster AGB star, and the remaining stars are helium burning clump star members of the cluster. The only dissents come in the proper motions for four stars from Kharchenko et al. (2013), as mentioned earlier.

Determination of asteroseismic masses depends on the accuracy and precision of the photometric data used to determine the parameters ν_{\max} and $\Delta\nu$, and of the method used to determine T_{eff} . Our calculations used the maximal *Kepler* datasets to reach precisions better than the previous determinations of Stello et al. (2011a) and Molenda-Żakowicz et al. (2014). Because the uncertainty on any individual star’s mass is relatively large (no less than about 5% even in our study), cluster giants are generally used as an ensemble to improve the precision of the mass measurement, which in turn provides the asteroseismic constraint on the age of the cluster (e.g., Basu et al. 2011). We have also improved the situation here by identifying all of the cluster giants: both Stello et al. and Molenda-Żakowicz et al. studied 5 giants. As

for T_{eff} , Stello et al. used photometric color- T_{eff} relations, and so were subject to systematic errors involving the poorly known cluster reddening and metallicity at the time. Stello et al. (2011a) derived a mean mass of $2.35 \pm 0.04 M_{\odot}$ from a shorter dataset for five stars in this sample. Molenda-Żakowicz et al. (2014) used spectroscopic T_{eff} and derived a mean mass of $2.12 \pm 0.14 M_{\odot}$.

After calculating T_{eff} using the more recent low value for reddening [$E(B - V) = 0.07 \pm 0.02$; see §1.1] and $V - K_s$ colors (employing Ramírez & Meléndez 2005), the mean mass determined from the asteroseismic relations is $\bar{M} = 2.28 \pm 0.03 \pm 0.04 M_{\odot}$, where the uncertainties are the error in the mean and the systematic uncertainty due to the reddening, respectively. The change in the reddening value largely accounts for the difference with the Stello et al. (2011a) value. As seen in Table 8, our photometric temperatures agree quite well with the spectroscopic values of Molenda-Żakowicz et al. (2014). In addition, we found that the three stars (KIC 9655167, 9716090, and 9776739) with the lowest masses calculated by Corsaro et al. (2012) from the asteroseismic observables are here found much closer to the mean for the other clump stars with these new values. (This is due to large changes of 4–8% in either the ν_{max} or $\Delta\nu$ observables for these stars.) The improvements underline the idea that the measurements for giants in the open clusters NGC 6791 and NGC 6819 should be revisited with the full *Kepler* datasets.

The reader should keep in mind that the clump phase, unlike the red giant branch (RGB) phase, is long enough that a mass range of at least a few hundredths of a solar mass is expected among the stars there, according to models. When that is coupled with a small sample of red clump stars as it is in NGC 6811, the average mass does not constrain the cluster age as strongly as it would with a comparable number of giants in an older cluster. Asteroseismic radii have higher precision than asteroseismic masses (2–3% versus 6–7% random uncertainty), and there is some dependence of the minimum clump star radius on age. For the six clump stars, we find weighted average values $\bar{M}_{RC} = 2.24 \pm 0.03 \pm 0.04 M_{\odot}$ and $\bar{R}_{RC} = 8.59 \pm 0.12 \pm 0.05 R_{\odot}$, where the quoted uncertainties are again random and systematic (due to reddening).

Although there are limited choices for comparisons with models, it is important to compare the asteroseismic inferences with predictions from stellar evolution utilizing our knowledge of the characteristics of the eclipsing binary stars. In Fig. 7, there is reasonable agreement with an age near 0.9 Gyr using PARSEC models. This age is younger than implied by the eclipsing binary, which can be interpreted as saying that the asteroseismic masses for the clump stars are larger than expected from the main sequence. There are potential systematic effects in the models that can affect this comparison, however. The reddening affects the asteroseismic masses more than the radii, so that a lower reddening moves the stars toward larger ages. Metallicity errors also affect the model masses more than radii (compare the solid and dotted lines in Fig. 7), in the sense that higher metallicity leads to larger ages. On the physics side, a larger mixing length parameter, for example, can reduce the computed radii of red clump stars (Yang et al. 2010). The scaling relations used to calculate the radii may also need to be

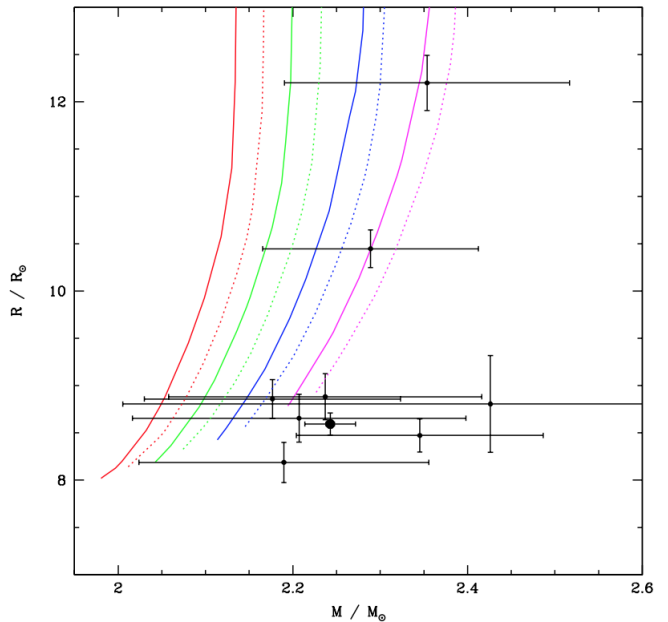


Figure 7. Asteroseismic mass-radius plot for helium-burning stars in NGC 6811, with the weighted average for the clump stars ($R < 9R_{\odot}$) shown with the large point. Models have ages of 0.9, 1.0, 1.1, and 1.2 Gyr (from right to left) for PARSEC (Bressan et al. 2012) isochrones, and have been restricted to helium burning phases for clarity. Solid lines use $Z \approx 0.0137$, and dotted lines use $Z \approx 0.0167$.

modified to apply accurately to red clump stars. Because the $\Delta\nu$ parameter relates to sound speed within a star, and because red clump stars have different structure than the red giant branch stars to which the scaling relations are usually applied, models indicate that $\Delta\nu$ is systematically higher for clump stars compared to giants with the same mean density (Miglio et al. 2012). However, models indicate that a clump star’s $\Delta\nu$ value is a more accurate indicator of its average density than it is for a giant (for example, see Fig. 4 of Sharma et al. 2016), and corrections to the scaling relations are more important for RGB stars. For RGB stars that have been studied in other *Kepler* clusters, there are indeed signs that uncorrected asteroseismic masses are overestimated (Brogaard et al. 2012; Sandquist et al. 2013). With a greater degree of constraint on the age of NGC 6811 from further study of the binary stars, the need for such corrections will be more strongly addressed.

4.1.2. The Main Sequence Turnoff and Pulsating Stars

Because a detailed membership study has not been completed for stars around the cluster turnoff, we need to identify the ones that should be used to delineate the evolutionary sequence for single stars. As a first step, we briefly review evidence for binarity among the brighter cluster stars in order to identify systems that could confuse the location of the single-star evolutionary sequence. A handful of binaries can be identified from their eclipses (Slawson et al. 2011). In the cases below, the proper motion indicators agree on cluster membership, but radial velocities were discrepant from the mean. They are therefore possible cluster members. KIC 9655187/Sanders 110 and KIC 9655346/Sanders 127 are known short-period eclipsing binaries, easily explaining

their radial velocity values. KIC 9716456/Sanders 159 has no radial velocity measurements, but is also a short-period eclipsing binary. KIC 9533489/Sanders 256 is a long period (197.15 d) eclipsing system with only one obvious eclipse that falls near the bluest part of the cluster main sequence, so that there is a good chance of cluster membership if the primary star dominates the photometry. KIC 9656397 was not identified in the Kepler Eclipsing Binary Catalog, but it shows two distinguishable eclipses during each 204.74 d cycle, and we have unpublished radial velocities showing that the system velocity matches the cluster mean. Finally, there are two fainter binaries without proper motion measurements. KIC 9655129 is a short-period eclipsing system, and KIC 9837544 is a longer period (71.662 d) binary. In both cases, the photometry puts them well to the red of the cluster main sequence, in spite of some support for membership from proper motions.

In NGC 6811, we can make use of an additional piece of circumstantial evidence that can argue for cluster membership: pulsation. We roughly translated the empirical boundaries of the δ Sct and γ Dor instability strips shown in Uytterhoeven et al. (2011) into the color magnitude diagram using VandenBerg & Clem (2003) color-temperature relations, assuming $[\text{Fe}/\text{H}]=0$, $E(B - V) = 0.07$, and $(m - M)_V = 10.33$. Although there are significant uncertainties in all of the quantities involved in making this translation (including the position of these empirical boundaries in T_{eff} and $\log g$), Figure 8 shows that cluster stars at the turnoff and redder can realistically be expected to be pulsating stars. This observation has been made previously by Frandsen & Arentoft (1998) and Luo et al. (2009), but the existence of *Kepler* photometry allows us to identify pulsators at quite low amplitude levels.

δ Sct and γ Dor stars in the NGC 6811 field have been previously identified in ground-based (van Cauteren et al. 2005; Luo et al. 2009) and *Kepler* (Debosscher et al. 2011; Uytterhoeven et al. 2011; Tkachenko et al. 2013) data. Uytterhoeven et al. focused on these two groups throughout the *Kepler* field, as well as hybrids showing frequencies belonging to both types. Debosscher et al. probabilistically categorize variable stars based on Fourier decomposition of *Kepler* quarter 1 data, though those authors found in a previous paper (Debosscher et al. 2009) that their δ Sct and β Cep classifications overlapped frequently — most of the stars they identify as β Cep in the NGC 6811 field are actually δ Sct. To produce a clean list of pulsators, we therefore examined the *Kepler* light curves of all of the stars near the turnoff and identified the type of variation using the frequency spectra.

To compute spectra, we downloaded the largest contiguous set of short cadence data when available, and long cadence data when not. Either type of data allows us to examine γ Dor frequencies ($f < 5$ c/d or 58 μHz). Long cadence data probes δ Sct below the Nyquist frequency ($f \approx 24.5$ c/d or 0.14 mHz), with some strong super-Nyquist frequencies potentially reflected in the spectrum as well (Murphy et al. 2013). We used Period04 software (Lenz & Breger 2005) to prewhiten the data successively after identifying and subtracting the highest-amplitude frequency remaining. Table 9 lists the stars with observed pulsation. A comparison of Tables 9

and 10 shows that stars with detectable pulsation constitute the majority falling within the expected instability strips.

We plan to discuss the spectra in more detail in an upcoming paper, but we comment on a few aspects of the pulsations that are relevant to establishing their cluster membership. Our understanding of the frequency structure of δ Sct stars is still limited, but gross features may reveal important information. For example, we expect the radial fundamental mode (if excited) to be near the lower frequency limit for δ Sct stars, although this is complicated by rapid rotation and the possible excitation of gravity or mixed modes. Based on dynamical timescale arguments, we should also expect that less luminous stars in NGC 6811 will be significantly more dense and would tend to have their pulsation modes shifted to higher frequencies ($f = \sqrt{\rho/\rho_{\odot}}/Q$, where Q is the pulsation constant for the mode). We plot the strongest observed frequencies for each δ Sct star as a function of V magnitude in the right panel of Fig. 8. A large proportion of the strongest frequencies fall approximately where predicted for the radial fundamental mode ($Q = 0.033$ d) using average densities derived from fitted isochrones, or using the period-luminosity relation for the fundamental mode of high-amplitude δ Sct stars with Hipparcos parallaxes (McNamara et al. 2007). These stars are found from the faint red end of the sample up to near the estimated blue end of the instability strip, consistent with the expectation that the fundamental mode is not excited at the blue edge (Pamyatnykh 2000). We believe this, along with the proper motions and color-magnitude positions of the stars, is good evidence that these stars are cluster members.

Many of the brighter stars have pulsation frequencies that are inconsistent with the radial fundamental mode or the first overtone radial mode (theoretically expected to have a period ratio of $P_1/P_0 = f_0/f_1 \approx 0.772$ with the fundamental). These frequencies can be found near the dashed line in the right panel of Figure 8. Although most of the faintest stars only have long cadence *Kepler* observations, and high frequency pulsations would be above the Nyquist limit, several stars with $V > 12.6$ have identifiable frequencies there.

Based on these observations, we derived an apparent distance modulus by fitting these data with the McNamara et al. (2007) period-luminosity relation. We restricted the sample to stars with strong frequencies nearest the expected value of the radial fundamental mode, although it is likely that physical processes (like rotational splitting for the higher frequency modes) would shift the frequencies that are actually excited. We note that binary companions to these stars would tend to bias their V magnitudes higher than they should be, and could cause us to underestimate the distance modulus. We compare the resulting distance modulus $(m - M)_V = 10.37 \pm 0.03$ with the results of the binary modeling in the next section.

In the remainder of this section, we discuss the membership of stars in different portions of the main sequence in preparation for using the color-magnitude diagram in model comparisons and age determination.

Stars brighter than the most heavily populated part of the main sequence ($V \lesssim 11.4$) are potentially impor-

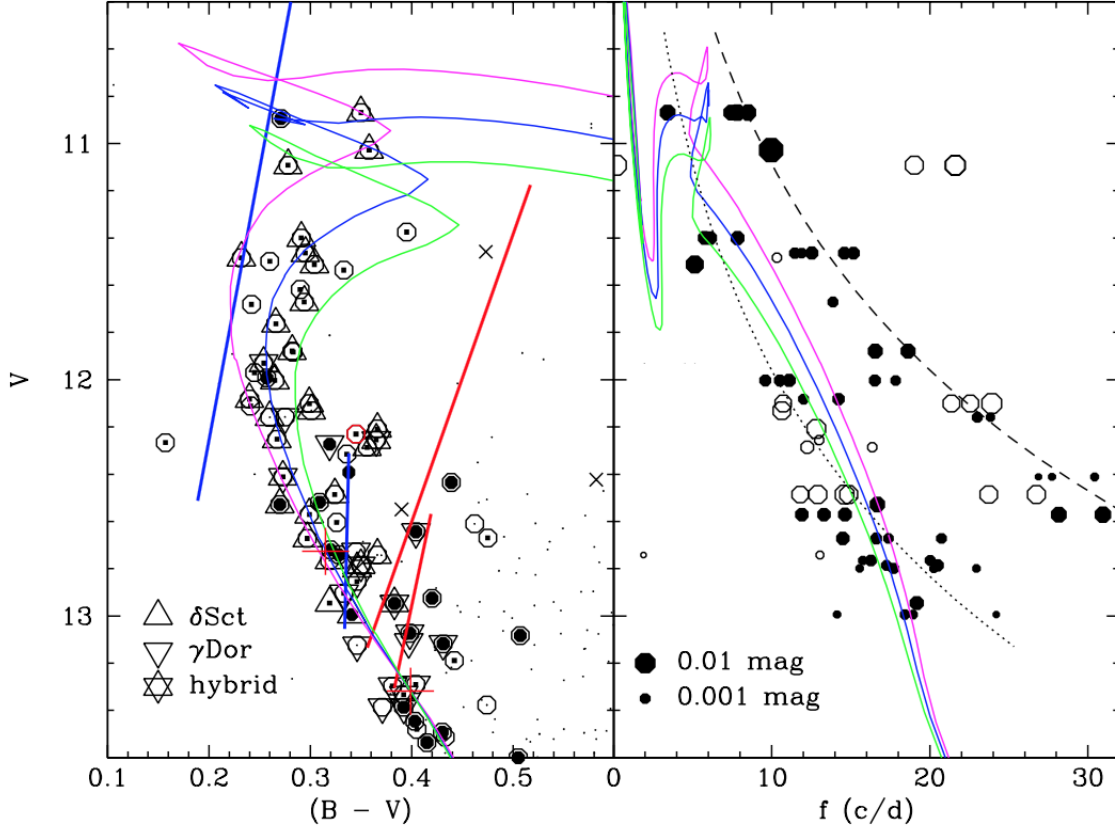


Figure 8. *Left panel:* Color-magnitude diagram for pulsating stars of δ Sct, γ Dor, or hybrid types in NGC 6811. Empirical instability strip boundaries are from Uytterhoeven et al. (2011) translated using $(m - M)_V = 10.33$ and $E(B - V) = 0.07$. The components of KIC 9777062 are shown with +, and radial velocity non-members are shown with \times . Isochrones are from the PARSEC (Bressan et al. 2012; $Z = 0.0137$) sets for ages of 0.9, 1.0, and 1.1 Gyr. *Right panel:* The highest amplitude modes (> 0.5 times the amplitude of the strongest) δ Sct stars versus V magnitude. The dotted line is the period-luminosity relation of McNamara et al. (2007), and the dashed line is the same relation with the frequency doubled. The colored lines are the PARSEC isochrones with average density used to predict the fundamental mode frequency, assuming $Q = 0.033$ d. Likely photometric binaries are shown with open symbols.

tant because they could trace the evolution at the time of core hydrogen exhaustion and constrain physical processes (like convective core overshooting) that affect the evolution. At the same time, unidentified binaries or blue stragglers can easily complicate model comparisons. Among these bright main sequence stars, the most important is probably KIC 9777532/Sanders 247 because it has unambiguous evidence of membership and no evidence of binarity. If its photometry is truly representative of a single star, it probably resides on the blue hook at the end of the main sequence isochrones. The other stars that have radial velocity membership information in addition to proper motions are KIC 9655177/Sanders 108, KIC 9716385/Sanders 136, KIC 9655543/Sanders 172, and KIC 9594857/Sanders 205. Three of these stars (S108, S136, S205) have been identified as δ Sct variables, and additional information on their interiors might be gleaned from their pulsations in the future. But among these stars, S136's pulsations stand out with an unusually high frequency in the δ Sct regime ($f \approx 22$ cycles per day). If its photometry is the result of being part of a nearly equal-mass binary, its pulsation frequency would be more in line with fainter cluster stars. Four radial velocity measurements to date (Frinchaboy & Majewski 2008; Meibom) show a large amount of velocity variability consistent with this. More velocity observations

are warranted for this star. S205 shows signs of velocity variability in the observations of Molenda-Żakowicz et al. (2014, 2 observations) and Frinchaboy & Majewski (2008, 1 observation), indicating that it is a likely single-lined spectroscopic binary (SB1). S108 only has one radial velocity observation (Frinchaboy & Majewski 2008), but it deviates from the cluster mean by about 15 km s^{-1} . So S247 appears to be the most likely single cluster member among these stars.

For stars on the main sequence above the cluster turnoff ($11.4 < V < 12$), there is a fair amount of scatter in the CMD that obscures the single star evolutionary sequence. In this group we can only identify one star (KIC 9716220/Sanders 113) that is a member by all criteria (radial velocity, proper motion, and pulsations), although it shows signs of velocity variability. Three other stars (KIC 9655055/Sanders 86, KIC 9655422/Sanders 144, and KIC 9655444/Sanders 149) are proper motion members and pulsators, but each shows velocity variability. Two additional stars (KIC 9655005/Sanders 77 and KIC 9655382/Sanders 134) are proper motion members and lack detectable pulsations. Both appear to be radial velocity members, but KIC 9655005 shows velocity variability while KIC 9655382 does not. The remainder of the stars in this range are eclipsing binaries, have radial

velocities that deviate from the cluster mean and could be spectroscopic binaries (S75, S87, S121, S161, S188, S230), or have detectable light travel time effect on δ Sct pulsations (S87; detected using the method of Murphy et al. 2014). Thus, we will restrict ourselves to at most 6 stars in this range of magnitudes. More precise CMD age constraints will require radial velocity study of candidate members here because this is where the isochrones start to separate most strongly.

Below the turnoff to the faint end of the instability strips for δ Sct and γ Dor stars ($12 < V \lesssim 13.4$), there are fewer published radial velocities for making membership and binarity judgements, but we can make better use of CMD position to eliminate binaries with bright secondary stars. The faintest δ Sct stars that are likely members have $V < 13$, while we find γ Dor stars down to $V \approx 13.4$.

Before moving on to a discussion of age and model comparisons, we return to the stars in the eclipsing binary. The deconvolved photometry of the two components of KIC 9777062 are plotted in Fig. 8, and their positions are consistent with other likely cluster single-star members. Because the stars appear to fall within the δ Sct and γ Dor instability strips respectively, we searched for evidence of pulsation in the light curve. We used short cadence *Kepler* data from the entirety of quarter 10, and subtracted the best fit model of the eclipses. The spectrum (Fig. 9) shows no evidence of δ Sct frequencies (> 5 cycles per day), but there are some low frequencies that may be associated with γ Dor pulsation. The amplitudes are about 0.25 millimag for the two strongest modes (0.6133 and 0.9525 c/d). The small amplitude of the modes (about an order of magnitude smaller in size than the secondary eclipse) means that they affect the eclipse light curves minimally. The pulsations probably result from the secondary star because the primary star appears to be well outside the estimated position of the γ Dor instability strip. As the pulsations are coherent, we investigated whether frequency modulation due to the binary orbit could be measured and used to identify which of the binary components is oscillating. Because we have characterized the binary orbit, we can predict the amplitudes of the sidelobes of the dominating observed oscillation modes in the power spectrum (Shibahashi & Kurtz 2012) and these are far too low to be measurable. We also tested whether any phase shift could be measured (Murphy et al. 2014) when fitting frequencies of the strongest modes to the light curve and isolating different orbital phases in the light curve, but we did not find any signal. However, we note that during the primary eclipse the light curve with the best-fit model subtracted show slightly increased scatter compared to the out-of-eclipse variation, which we take as indication that the pulsations originate from the secondary component. Although the primary star does not appear to be a pulsating star itself, the very precisely determined masses and radii for both stars can be used to predict masses and radii for other NGC 6811 pulsators.

4.2. The Cluster Age and Distance Modulus

To make the connection between cluster age and stellar characteristics, theoretical models are necessary, and systematic differences in the input physics or chemical composition will affect the inferred age. Table 7 summarizes

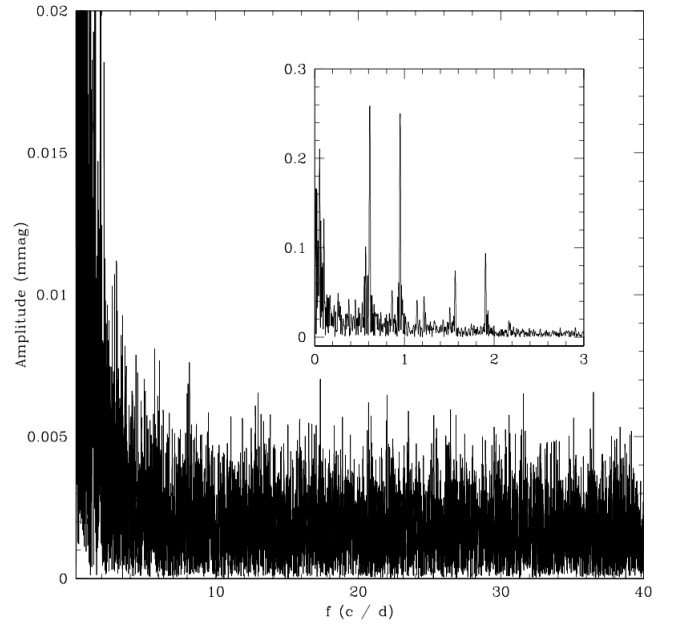


Figure 9. The amplitude spectrum for KIC 9777062 after subtraction of model eclipses from the light curve. The inset shows a zoom on the detected low frequencies.

some of the more important physics inputs in presently available model sets. To highlight physics differences, we use a common set of ages for all of the comparisons between sets of theoretical isochrones, and very nearly the same heavy element abundance Z . It is important to remember that there are potential systematic errors in our choice of Z , both due to uncertainties in the measured abundances relative to the Sun, and due to continuing uncertainty over the Sun’s heavy element abundances. Even when forcing the models to have a common heavy element abundance, different helium abundances will be present in the models, both because of the need to calibrate the models to the Sun for the included physics and because of different assumptions about the galactic helium enrichment rate (usually parametrized as $\Delta Y/\Delta Z$). For the models used here, the differences between the highest and lowest abundances are modest (0.02 in Y).

Because the stars in the eclipsing binary KIC 9777062 are relatively slow rotators compared to the majority of single stars in their mass range, diffusion may play an important role in our discussion. The Victoria-Regina isochrones employed here (VandenBerg et al. 2006) do not include diffusion, although their more recent models have implemented helium diffusion. For the PARSEC isochrones (Bressan et al. 2012), diffusion is turned off if the star is more massive than $1.60M_{\odot}$ (which leaves out the primary star and turnoff stars in NGC 6811) or when the mass of the surface convection zone falls below $0.005M$, where M is the mass of the star. For the Dartmouth isochrones (Dotter et al. 2008), diffusion is inhibited in the outermost $0.005M_{\odot}$, and ramped up to full strength $0.01M_{\odot}$ below the photosphere (Chaboyer et al. 2001). For the Yonsei-Yale isochrones (Demarque et al. 2004), helium diffusion is allowed to run at full strength.

As for uncertainties in convection physics, we briefly mention core overshooting and the mixing length. Core

Table 7
Summary of Relevant Inputs for Model Isochrone Sets

Isochrone	Z	Y	Diffusion?		Overshoot λ_{OV}/H_P	Mixing Length α_{ML}
			Y	Z		
Dartmouth	0.01375	0.2659	Y	Y	0.20	1.94
PARSEC	0.01370	0.2726	N/Y ^a	N/Y ^a	~ 0.25	1.74
Victoria-Regina	0.01250	0.2629	N	N	^b	1.90
Yale-Yonsei	0.01370	0.2574	Y	N	0.20	1.74

^a PARSEC isochrones assume no diffusion for a star with the mass of the primary star in KIC 9777062, but diffusion acting for a star with the mass of the secondary.

^b Victoria-Regina models use a different algorithm for convective core overshooting, so it is difficult to directly compare to the other sets.

overshooting generally does not have a significant effect on observable properties until stars are nearing hydrogen exhaustion: a larger amount of overshooting prolongs a main sequence star’s life and affects how rapidly the star needs to adjust to hydrogen exhaustion. Differences here affect comparisons in the CMD at the brightest part of the main sequence and on the subgiant branch, but should not affect the $M - R$ comparison for our binary. The mixing length ($\Lambda = \alpha_{ML} H_P$, where H_P is the pressure scale height) has its largest effects on the properties of surface convection zones. Although the stars near the turnoff of NGC 6811 (including the stars of our binary) should have very low surface convection zone masses, the evidence is that surface convection is still present in the fainter half of the instability strip at least and that the convection might be more turbulent than for cooler stars.

4.2.1. Mass-Radius ($M - R$) Comparison

As stated earlier, a comparison with models in the mass-radius plane avoids common uncertainties that plague CMD comparisons: reddening, distance, and color- T_{eff} transformation uncertainties. Fig. 10 shows the comparison with the components of KIC 9777062 in the $M - R$ plane. Isochrones from different groups look similar, but there are interesting differences for each of the binary components. For the primary star, the Dartmouth isochrones (Dotter et al. 2008) are noticeably offset toward smaller stars for a given age compared to PARSEC (Bressan et al. 2012), Victoria-Regina (VandenBerg et al. 2006), and Yonsei-Yale (Demarque et al. 2004) isochrones. For the secondary star, the Dartmouth models again have the smallest radii at a given age, but the Victoria-Regina models predict significantly larger radii than the PARSEC and Yonsei-Yale models. The differences imply that there are some significant differences in the input physics being used. We have not found clear reasons to explain the differences between model radii, however. For example, if helium abundance was the dominant influence on the model radii, the PARSEC models should have been smallest and the Yale-Yonsei should have been largest, which is not seen. The Dartmouth and Yonsei-Yale isochrones are the only ones that incorporate helium diffusion at present, but these are not models with the largest radii (due to higher opacity in the surface layers). Because of the uncertainties in model radii, we will consider the dispersion to be at least partially representative of the systematic errors involved in deriving the age. This comes to approximately ± 0.04 Gyr for the primary star, and ± 0.10 Gyr for the secondary. If metallicity uncertainties are considered (as in

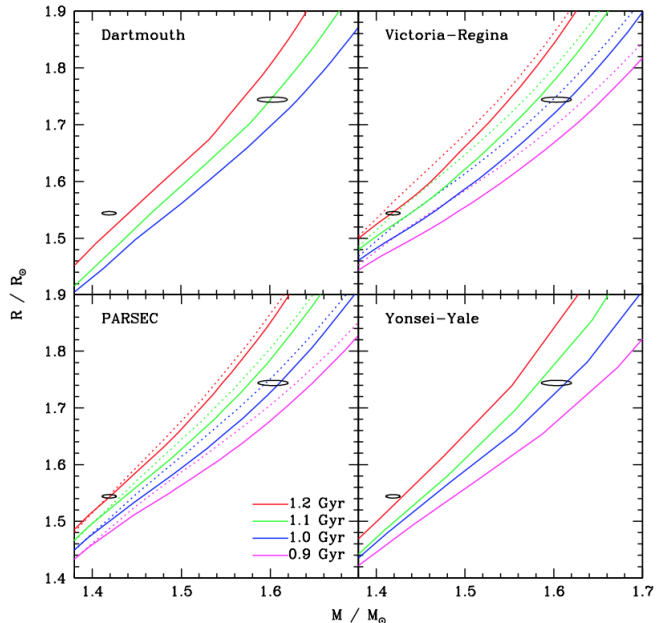


Figure 10. Mass-radius plot for the members of KIC 9777062 with 1σ uncertainty ellipses. Models have ages of 0.9, 1.0, 1.1, and 1.2 Gyr (from bottom to top) for Victoria-Regina (VandenBerg et al. 2006), PARSEC (Bressan et al. 2012), and Yonsei-Yale (Demarque et al. 2004) models, while the Dartmouth (Dotter et al. 2008) models have ages of 1.0, 1.1, and 1.2 Gyr. Solid line isochrones use $Z \approx 0.0137$ in all panels but Victoria-Regina. In the PARSEC panel, the dotted lines show $Z = 0.0167$. In the Victoria-Regina panel, our preferred Z is midway between the solid and dashed lines ($Z = 0.0125$ and 0.015 , respectively).

the PARSEC panel of Figure 10), there is an additional systematic uncertainty of about 0.05 Gyr for both stars.

Although the mass and radius measurement uncertainties are larger for the primary star in the binary, the two stars produce age estimates with similar precision (about 0.05 Gyr) for a given set of isochrones because the primary star’s characteristics place it where there is greater separation between isochrones. The age estimates produced by the separate components of the binary, however, are different by about $2 - 3\sigma$, with the secondary returning an age that is about 0.15-0.20 Gyr higher than that for the primary.

Regarding the different age estimates returned by the two binary components, initial helium abundance can modify the shape of the isochrone (Brogaard et al. 2011). We do not consider this to be the most likely explanation because NGC 6811 stars show elemental abundances that are otherwise quite close to solar abundances (with

the exception of barium; Molenda-Żakowicz et al. 2014). If heavy element and helium abundances are connected ($\Delta Y/\Delta Z$ is a constant, for example, as is often assumed), the small super-solar metallicity would produce a minor enhancement in the helium abundance ($\Delta Y \sim 0.001$) on its own.

Main sequence stars having massive surface convection zones in short-period eclipsing binaries have been shown to have radii that are inflated by as much as 10% above theoretical expectations (Torres et al. 2006), possibly because magnetic activity helps inhibit convective motions and makes the convection less efficient. It can be argued that this kind of effect should be minimal in the KIC 9777062 system: the orbital period is substantially larger than in affected binaries ($P \lesssim 3.5$ d), and there should be a very low-mass surface convection zone for the secondary star ($< 10^{-3} M_{\odot}$) and an even less massive surface convection zone for the primary star. Convection should be less efficient in the very shallow convection zone of the primary due to radiative losses, and this is also unlikely to help produce a smaller radius.

We can also examine whether there are effects on the radius related to physics involved in the Am/Fm phenomenon. One empirical approach that can be used to examine this question is to look at precisely measured eclipsing binary star systems that include Am/Fm stars. In the interest of the paper’s readability, we have put this discussion into an appendix. Our conclusion is that the properties of the secondary star in the $M - R$ plot for KIC 9777062 are likely to be the most trustworthy for determining the age because it does not show the extreme abundance anomalies that the primary star does. However, the properties of the primary stars in this and other binaries are not understood at present, and may be subject to physics that is not being included in models. The model isochrones themselves do not agree at the level we need to be able to derive a confident absolute age for the cluster, and the differences between models cannot be attributed confidently to one physics input (like diffusion) or another. We are forced to conclude that more theoretical and observational effort needs to be exerted to understand stellar radii in this range of masses.

Before moving on to color-magnitude diagram comparisons, we can use the stellar radii in concert with a T_{eff} estimate to compute the luminosity of each star. With an additional bolometric correction, the absolute magnitude and apparent distance modulus can be calculated. We utilized bolometric corrections in V from Casagrande & Vandenberg (2014) along with the model radii and spectroscopic temperature estimates from §3.3 to find $(m - M)_V = 10.47 \pm 0.09$ and 10.47 ± 0.06 , respectively for the primary and secondary components. The largest contributor to the uncertainty in these distance moduli by far is the temperature. The averaged distance modulus is $(m - M)_V = 10.47 \pm 0.05$.

The binary star distance measurements are modestly outside the 1σ uncertainty ranges from previous determinations. Molenda-Żakowicz et al. (2014) derive $(m - M)_V = 10.29 \pm 0.14$ using a combination of spectroscopic and asteroseismic information for 5 red clump stars, and our own re-examination of the giant sample (omitting KIC 9409513) gives $(m - M)_V = 10.31 \pm 0.04$, where the uncertainty estimate is the standard deviation

of the measurements (to better represent the likely systematic nature of the errors in T_{eff} measurements). Our analysis of cluster δ Sct stars produced a measurement of 10.37 ± 0.03 . Janes et al. (2013) quote a best estimate $(m - M)_V = 10.22 \pm 0.18$ from Bayesian comparison of isochrones with color-magnitude diagrams, but there are systematic uncertainties relating to the choice of an isochrone set. For example, they derive $(m - M)_V = 10.13 \pm 0.19$ using Yale-Yonsei isochrones, but 10.31 ± 0.11 using Padova isochrones. In addition, their analysis found lower metallicities than have been found spectroscopically, and this would lead them to overestimate the luminosity and derive systematically smaller distance moduli. At the same time, if our spectroscopic temperatures for the binary are overestimated by less than the uncertainties given above, our distance moduli would come into better agreement.

4.2.2. Color-Magnitude Diagram (CMD) Comparisons

Any comparison in the CMD using just the distance modulus and reddening to shift the theoretical isochrones will also be subject to issues involving inaccuracies in the color- T_{eff} transformations, but we do a preliminary comparison in Fig. 11 using the distance modulus derived from the binary system and a reddening that moves the main sequence into approximate agreement with the fainter star in the binary. The four sets of isochrones appear to agree on an age of 0.9–1.0 Gyr, and this includes the potentially single star at $V \approx 10.9$. That star (KIC 9777532/Sanders 247) may be a legitimate cluster subgiant. If so, it can give us good leverage on the age from the CMD. More study is needed in order to determine whether its CMD position is affected by an undetected companion, however.

Because we have mass measurements for the KIC 9777062 stars, we can force isochrones to fit their CMD positions, thereby constraining isochrone positioning further. This should also minimize the effects of uncertainties in reddening, distance modulus, and color-temperature relations. A first comparison to make is whether the models match the observed magnitude separation for the measured star masses. The observed $\Delta V = 0.586 \pm 0.021$ is smaller than the model predictions by about 0.07 mag, and this cannot be explained by calculated uncertainties in the star masses or reasonable uncertainties in the age or metallicity of the cluster. As discussed in the previous subsection, this may be an indication that the physics implemented in the model isochrones is not adequately describing what is occurring in the primary star. Diffusion is a leading suspect in this case because of the Am nature of the primary. We therefore think that the most reliable comparison will be between the model isochrones and the secondary star. If most of the other stars near the turnoff of NGC 6811 do not show Am/Fm characteristics, then our CMD comparisons should also be valid. Tests of these assumptions are beyond the scope of this paper, but the analysis of other eclipsing binaries in the cluster would help. Lower-mass stars are expected to be less affected by diffusion due to their larger surface convection zones, and we predict that the properties of these stars relative to the secondary of KIC 9777062 will be in line with models.

Fig. 12 shows a comparison of isochrones to cluster star photometry for our restricted set of members that

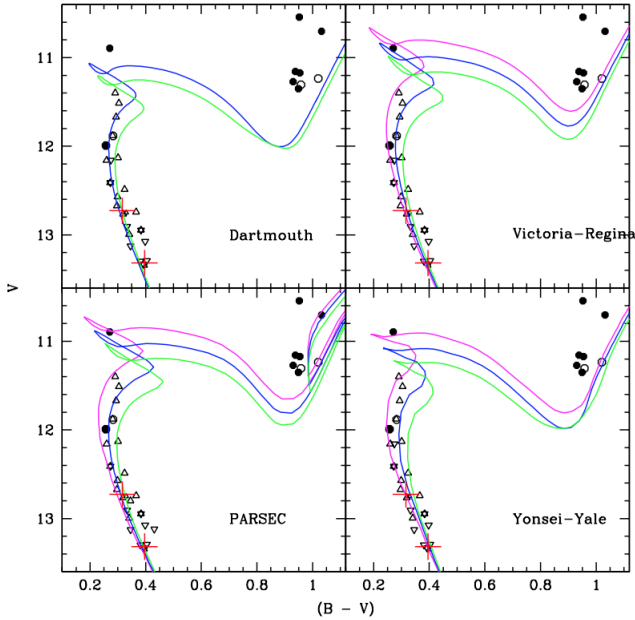


Figure 11. Color-magnitude diagram comparison for fixed reddening [$E(B - V) = 0.07$], distance modulus [$(m - M)_V = 10.47$], and metallicity. Model isochrones have ages of 0.9 Gyr (magenta), 1.0 Gyr (blue), and 1.1 Gyr (green) for Dartmouth ($Z = 0.0147$), Victoria-Regina ($Z = 0.0150$), PARSEC ($Z = 0.0147$), and Yonsei-Yale ($Z = 0.0147$) isochrones. Points have the same meaning as in Fig. 8.

are least likely to be binaries. For all of the isochrone sets, the bluest stars on the upper main sequence imply an age just under 1.0 Gyr. In the case of the Victoria-Regina, PARSEC, and Yonsei-Yale isochrones, the potential subgiant at $V \sim 10.9$ also indicates an age close to 1.0 Gyr, with good consistency between the three sets of models. The Dartmouth models imply a somewhat younger age, but that group does not currently tabulate isochrones for ages less than 1.0 Gyr. The magnitude and color shifts needed to force agreement with the secondary star range from $(m - M)_V = 10.27$ to 10.34 and $E(B - V) = 0.05$ to 0.08, where the PARSEC, Victoria-Regina, and Yonsei-Yale model values agree well and sit at the low end for both quantities.

Systematic uncertainties are always important considerations for age measurements, and we briefly discuss them here. Metallicity uncertainties, whether due to the cluster or to solar composition, affect the ages at the level of a few hundredths of a Gyr (see the PARSEC and Victoria-Regina panels of Figs. 10 and 12). There are a number of stellar physics uncertainties that could affect whether the isochrones truly represent observed stars near the turnoff. One of these is rotation (e.g., Brandt & Huang 2015), which is expected to extend the lifetimes of main sequence stars and make them appear more luminous. While the stars of the eclipsing binary should not be affected, ages determined from rotating turnoff stars would be biased toward younger ages. This effect is difficult to evaluate properly, and may require examination of spectroscopic rotational velocities for a large sample of the turnoff stars.

For most of our comparisons utilizing the components of KIC 9777062, we will be insensitive to the details of

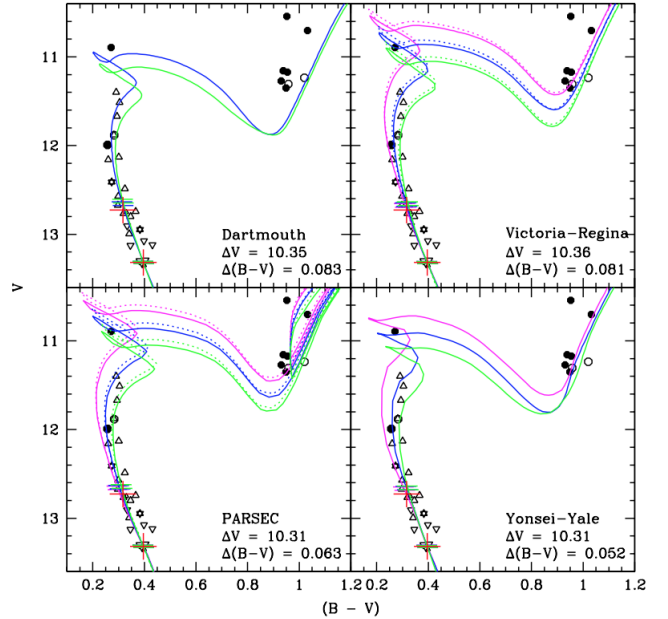


Figure 12. Color-magnitude diagram for selected probable members of NGC 6811 with isochrones shifted to match the mass and photometry of the secondary star of KIC 9777062. (Magnitude and color shifts are given in each panel.) All stars have proper-motion membership probabilities $P_{PM} > 0.50$ (Sanders 1971). Radial velocity members are shown with \bullet . Pulsating stars and the components of KIC 9777062 have the same symbols as in Fig. 8. Isochrones are from the Dartmouth (Dotter et al. 2008; $Z = 0.0137$), Victoria-Regina (VandenBerg et al. 2006; $Z = 0.0125$ and 0.0151 with solid and dashed lines), PARSEC (Bressan et al. 2012; $Z = 0.0137$, dotted lines show $Z = 0.0167$), and Yonsei-Yale (Demarque et al. 2004; $Z = 0.0137$) sets for ages of 0.9, 1.0, and 1.1 Gyr (magenta, blue, and green respectively). The predicted position of the primary star relative to the secondary for different isochrones are shown at $V \approx 12.6 - 12.7$.

convective core overshooting because this has its most observable effects near core hydrogen exhaustion or beyond. So at present, the photometry of the bright main sequence stars is our main constraint on this process. Without a more detailed survey of the radial velocities of turnoff stars to evaluate binarity, we cannot say much more than the cluster CMD seems to be consistent with overshooting in an amount of approximately 0.2 pressure scale heights, as is used in the Dartmouth, Yonsei-Yale, and PARSEC models.

4.2.3. Age Summary

Because we produced measurements covering a disparate set of techniques, it is worth summarizing the results and examining the degree to which the different techniques produce consistent results.

Asteroseismic masses and radii for clump giants in the cluster imply an age near 0.9 Gyr, but this estimate may suffer from significant systematic uncertainties, including the treatment of convection in the isochrones and the asteroseismic scaling relations used to calculate the radii.

The masses and radii measured for the stars in the eclipsing binary imply different ages, with the primary appearing younger than the secondary star (1.02 – 1.08 Gyr versus 1.17 – 1.25 Gyr). Because the primary star shows the Am metal-line phenomenon, we believe it is more likely to be experiencing physics effects (like diffusion) that are not properly represented in the models

used to interpret the age. If the two stars in the binary have lower metallicity than used in the model isochrones, this would also tend to slightly improve the agreement of the ages derived separately from each of them.

Age determinations from the CMD require some decision on how much the isochrones need to be shifted in magnitude and color. While fits are frequently done to derive distance, reddening, and age simultaneously, uncertainties in the color- T_{eff} relations assumed in the isochrones affect the validity of the inferred values. If we shift isochrones to match the V magnitude of the secondary star in the eclipsing binary at its measured mass, the implied distance modulus is in rough agreement with our independently derived values from fitting a period-luminosity relation to the cluster δ Sct stars and from asteroseismology of the giant stars. However, the preferred CMD age in this case appears to be near 1.0 Gyr (uncertainty around 0.05 Gyr), in disagreement with the secondary star mass-radius measurement. It should be remembered that the CMD age is dependent on our ability to isolate a sample of single stars that are brighter than the turnoff ($V \lesssim 12$). In a sparse cluster like NGC 6811, this is challenging, and more radial velocity and asteroseismic work can be done to verify that the stars in our sample do not have bound companions. In addition, if cluster stars have higher metallicity than used in the isochrones, the CMD age would move older. A higher metallicity makes the mass-radius ages of the KIC 9777062 stars disagree more, however, and leads to the conclusion that consistency in the ages cannot be achieved by simply assuming a different metal abundance.

5. CONCLUSIONS

We presented a detailed analysis of the first detached eclipsing binary member of the open cluster NGC 6811 containing stars near the turnoff. The primary star shows surface abundance anomalies consistent with being a metal-line Am star, and one of the stars (probably the secondary, based on its CMD position, radial velocity scatter, and increased photometric scatter during primary eclipse) is a γ Dor pulsating star. The indication of a convective blueshift for the primary star implies that it probably has a turbulent surface convection zone that is shallow enough to allow diffusive chemical separation and the Am phenomenon. The less massive secondary star does not show chemical peculiarities and shows a lower microturbulent velocity, implying that its surface convection zone goes deep enough to circumvent diffusive separation. Nearly all stars in well-measured binaries with masses between 1.3 and $1.55M_{\odot}$ appear chemically normal.

A surprising outcome of the measurement of the stellar masses and radii is that they indicate different ages, with the secondary star returning an age that is 15-20% larger than the primary star. In lower mass and shorter period binaries this kind of discrepancy has been attributed to induced magnetic activity and inhibition of convective energy transport that leads to a larger radius for the secondary star having a deeper convective zone. While the stars are rotating slowly and thereby show signs of tidal interaction, the orbital period is much longer than any binaries showing radius discrepancies among lower mass stars and the convection zones in these stars would

themselves be much lower in mass and less likely to be affected by magnetic activity. On the other hand, more than a third of Am stars in the fields observed by *Kepler* have been shown to have photometric variations that are likely due to spots (Balona et al. 2015). Further, there are other well-studied eclipsing binaries containing more massive Am stars that show similar patterns in their masses and radii. Regardless, we have yet to identify a convincing explanation why at least one of these stars seems to have an anomalous radius when compared with models.

Deeper study of other types of stars in the cluster may help clarify the picture. With the large number of δ Sct pulsating stars occupying the turnoff of this cluster, this binary and others provide the excellent opportunity to determine accurate masses for an ensemble of pulsating stars with extensive *Kepler* photometry in order to derive additional strong observational constraints on stellar models. One application we examined was the use of the period-luminosity relation for high-amplitude δ Sct stars with *Hipparcos* parallaxes to derive an independent measure of the distance modulus. A promising line of future research is the derivation of mean stellar densities from the equivalent of the large frequency spacing for these stars (Suárez et al. 2014).

We re-examined the sample of secondary clump and asymptotic giant stars in the cluster and re-analyzed their asteroseismic data from the main *Kepler* field. The small sample of clump stars (there are no first-ascent red giants) and the relatively large measurement uncertainties do not allow us to produce a tight constraint on the age, but the mass-radius values are consistent with a 0.9 Gyr age. A deeper analysis going beyond the observables $\Delta\nu$ and ν_{max} could further test the consistency of the asteroseismic results with measurements from the CMD, the main sequence pulsators, and the eclipsing binary stars.

At the end of this survey, we have not found a model of any age that is consistent with all of the observations. The results tend to break in to groups near 1.0 Gyr (the mass and radius of the primary of the eclipsing binary; photometry of turnoff stars when isochrones are pinned to the mass and photometry of the secondary star; the asteroseismic masses and radii of the secondary clump stars) or near 1.2 Gyr (the mass and radius of the secondary star). The distance moduli we have derived from the eclipsing binary and δ Sct stars also differ with each other at the 0.1 mag level, with the δ Sct result being closer to the isochrone predictions. There are significant differences between the predictions of different sets of isochrones and significant uncertainties that currently limit our ability to identify a preferred age and distance. Observations that would improve the situation include: further radial velocity study of the brightest main sequence stars (especially the subgiant candidate KIC 9777532) to find or rule out previously undetected binary companions; characterization of additional eclipsing binaries in the cluster; and establishment of more precise spectroscopic temperatures for turnoff stars. On the theoretical side, there is a need to identify the sources of the differences between sets of isochrones, and to test and improve the treatment of helium and heavy element diffusion. At the turnoff of NGC 6811, the mix of stars — with and without binary companions, and with different

rates of rotation — may be confounding our understanding more than we realize.

We thank the anonymous referee for comments that improved the presentation of the paper.

E.L.S. is grateful to the Stellar Astrophysics Centre at Aarhus University for their generosity and hospitality during his sabbatical stay, during which part of this work was completed. Funding for the Stellar Astrophysics Center is provided by the Danish National Research Foundation (grant agreement no. NDRF106) with research supported by the ASTERISK project (ASTER-oseismic Investigations with SONG and Kepler) funded by the European Research Council (grant agreement no. 267864). Our work has been funded through grant AST 09-08536 from the National Science Foundation and grant NNX13AC19G from the National Aeronautics and Space Administration to E.L.S. M.L. was supported as part of the Research Experiences for Undergraduates site at San Diego State University, funded by the National Science Foundation under grant AST-0850564 to E.L.S. K.B. acknowledges support from the Carlsberg Foundation and the Villum Foundation. We would also like to thank S. Brunner, E. Rich, C. Curtin, M. Lapid, J. Mascoop, and J. Pautzke for assisting in the acquisition of ground-based photometric observations, and staff and student support astronomers at the NOT (T. Augsteijn, A. A. Djupvik, T. Pursimo, J. Telting, F. S. Kiaerad, G. Barisevicius, J. Lehtinen, O. Smirnova, S. Geier, T. Kangas, J. Kajava, and Y. Martinez-Osori) for assisting in the acquisition of FIES observations.

We are very grateful to the *Kepler* team for the opportunity to work with such a precise and extensive dataset for detecting variable stars. This paper includes data collected by the *Kepler* mission. Funding for the *Kepler* mission is provided by the NASA Science Mission directorate. This research made use of the SIMBAD database, operated at CDS, Strasbourg, France; the NASA/IPAC Infrared Science Archive, which is operated by the Jet Propulsion Laboratory, California In-

stitute of Technology, under contract with the National Aeronautics and Space Administration; the WEBDA database, operated at the Institute for Astronomy of the University of Vienna; Astropy, a community-developed core Python package for astronomy (Astropy Collaboration, 2013); and the Mikulski Archive for Space Telescopes (MAST). STScI is operated by the Association of Universities for Research in Astronomy, Inc., under NASA contract NAS5-26555. Support for MAST is provided by the NASA Office of Space Science via grant NNX09AF08G and by other grants and contracts.

The HobbyEberly Telescope (HET) is a joint project of the University of Texas at Austin, the Pennsylvania State University, Stanford University, Ludwig-Maximilians-Universität München, and Georg-August-Universität Göttingen. The HET is named in honor of its principal benefactors, William P. Hobby and Robert E. Eberly.

Funding for SDSS-III has been provided by the Alfred P. Sloan Foundation, the Participating Institutions, the National Science Foundation, and the U.S. Department of Energy Office of Science. The SDSS-III web site is <http://www.sdss3.org/>. SDSS-III is managed by the Astrophysical Research Consortium for the Participating Institutions of the SDSS-III Collaboration including the University of Arizona, the Brazilian Participation Group, Brookhaven National Laboratory, Carnegie Mellon University, University of Florida, the French Participation Group, the German Participation Group, Harvard University, the Instituto de Astrofísica de Canarias, the Michigan State/Notre Dame/JINA Participation Group, Johns Hopkins University, Lawrence Berkeley National Laboratory, Max Planck Institute for Astrophysics, Max Planck Institute for Extraterrestrial Physics, New Mexico State University, New York University, Ohio State University, Pennsylvania State University, University of Portsmouth, Princeton University, the Spanish Participation Group, University of Tokyo, University of Utah, Vanderbilt University, University of Virginia, University of Washington, and Yale University.

APPENDIX

PHOTOMETRIC CALIBRATION

The field of the eclipsing binary KIC 9777062 was observed on 2012 Aug. 26, while three other fields (including the cluster center) were observed on 2013 Aug. 8. We observed Landolt standard fields SA 92, SA 110, and SA 114 as well as the open clusters NGC 6939 and NGC 6940 at airmasses ranging from 1.030 to 1.846. We used stars and standard values from Stetson (2000, Nov. 5, 2013 release) covering a color range $0 \leq (B - I) \leq 8$. In the course of the calibration, we discovered that the residuals of our photometry of the NGC 6940 field had a consistent trend with x position. Upon investigation, we found that this trend (a large 0.09 mag in full extent) appears to be in the Stetson standard magnitudes because we find it consistently in these two nights and others. We opted to use our own observations to recalibrate the NGC 6940 stars because we observed this cluster over a significantly larger range of airmass than our other standard fields and would therefore be in a better position to evaluate airmass-dependent terms in the photometric transformations below.

We derived instrumental magnitudes from aperture photometry conducted using DAOPHOT with curve-of-growth corrections derived using DAOGROW. The transformations to the standard system employed the equations

$$\begin{aligned} b &= B + a_0 + a_1(B - I) + a_2X, \\ v &= V + b_0 + b_1(B - I) + b_2X, \\ i &= I + c_0 + c_1(B - I) + c_2(B - I)^2 + c_3X, \end{aligned}$$

where b , v , and i are instrumental magnitudes, B , V , and I are standard system magnitudes, and X is airmass.

We compared our BV photometry with two previously published datasets, partly to provide an independent check of literature photometry and to test whether different photometric observations of this extended cluster could realistically

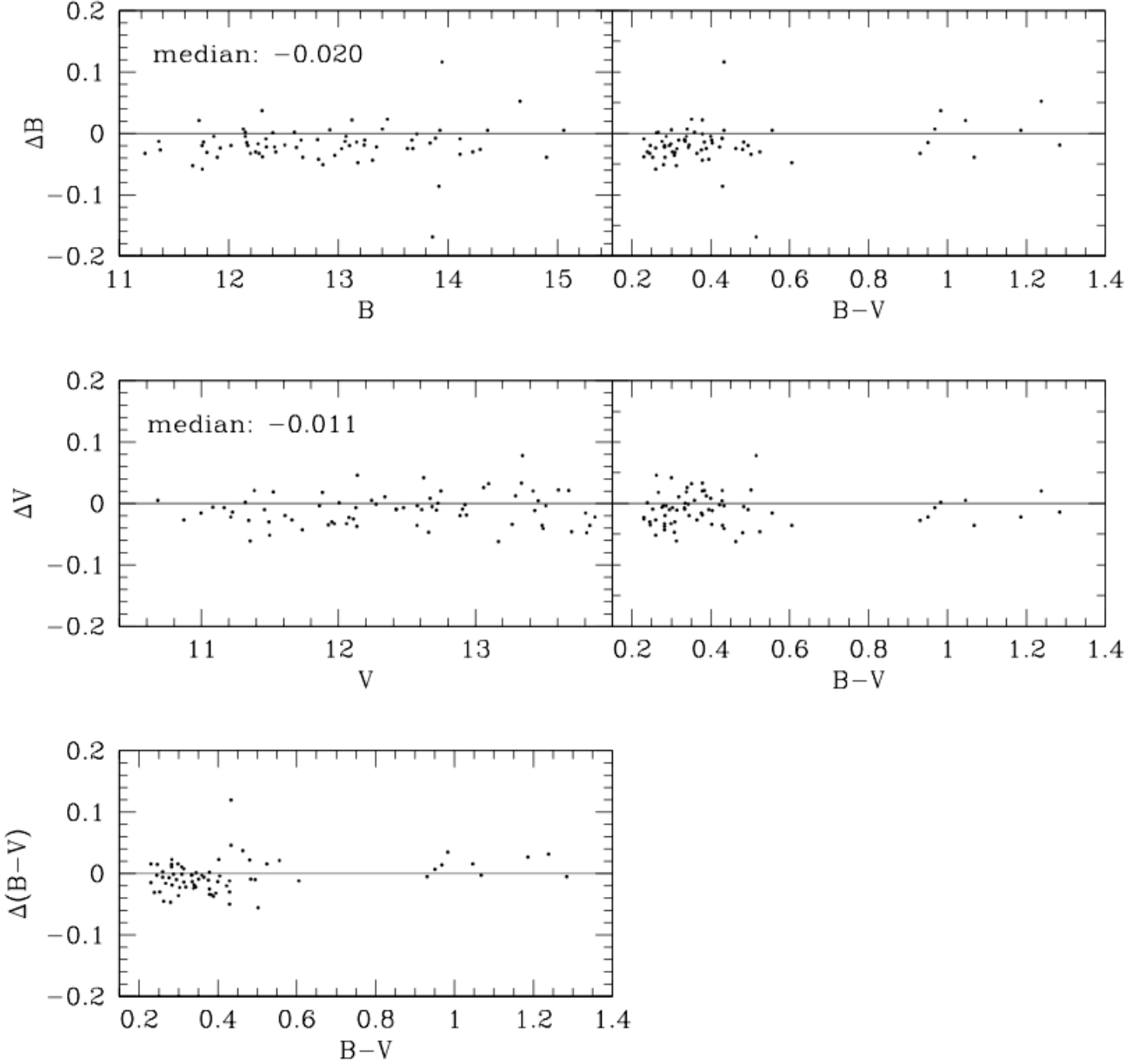


Figure 13. Differences between the BV photometry of Glushkova et al. (1999) and the present paper in the sense of (ours - theirs).

be combined together. Using 82 stars in common with the photoelectric photometry of Glushkova et al. (1999), we found median offsets (in the sense of our photometry minus theirs) of -0.020 and -0.011 mag in B and V , respectively. There were no signs of magnitude dependencies in the differences (see Fig. 13), and only a small sign of a trend in color residuals versus color (in the sense that giants tended to be slightly redder relative to the main sequence stars in our photometry).

We also compared with the photometry of Janes et al. (2013) and found good agreement (see Fig. 14). There were no indications of trends with magnitude, hints of a small trend of B magnitude with color, and slight trends of magnitude residuals with declination coordinate (most significantly, a variation of about 0.04 mag in B in the southernmost of our four fields, in the sense that our photometry gets systematically fainter with respect to Janes et al. as declination decreases). In their study and ours, the cluster was covered by tiling together multiple fields, but Janes et al. also made use of multiple telescope/instrument combinations. The section of the field that shows the greatest evidence of a position-dependent trend was their Hall telescope field from 2010. Based on this, we believe we have done a slightly better job of removing position-dependent trends, but the Janes et al. study has somewhat better signal-to-noise, as seen in reduced scatter among main sequence stars in Figure 15.

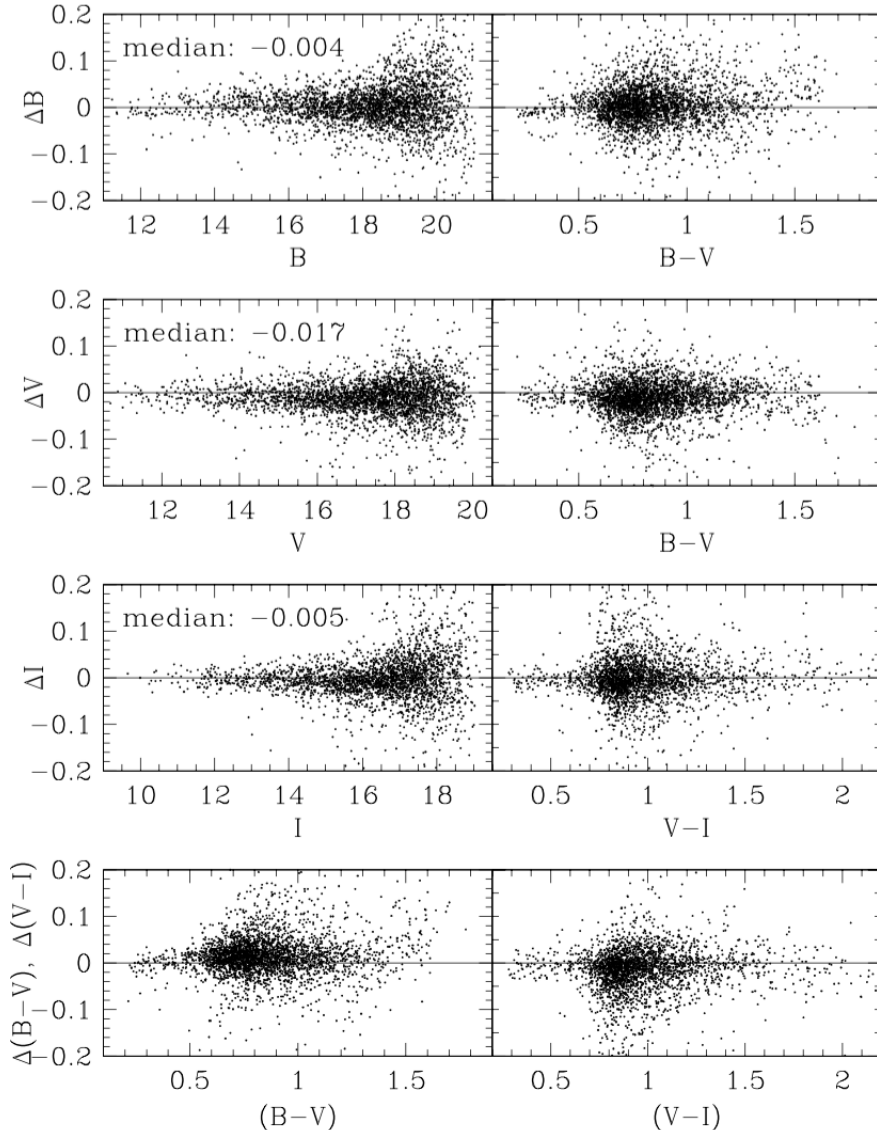


Figure 14. Differences between the BVI_C photometry of Janes et al. (2013) and the present paper in the sense of (ours - theirs).

MASSES AND RADII OF AM/FM STARS

We looked at systems in the compilation of Torres et al. (2010) that had stars in the mass range covered by these stars (approximately $1.4 - 2.4M_{\odot}$), supplemented with additional eclipsing Am binaries from more recent literature (Groenewegen et al. 2007; Southworth et al. 2011; Torres et al. 2012, 2015). Detached systems like these should contain stars with equal age and bulk composition (although the surface composition may be greatly affected), so that each pair *should* lie on the same isochrone if the Am/Fm phenomenon is unimportant. In Fig. 16, we plot a $M - R$ diagram for these stars using isochrones of NGC 6811 metal content. While not universally true (for stars near the masses of the KIC 9777062 components, see HY Vir and V501 Mon), there are a number of systems with a line connecting the components that appears to have a shallower slope than the isochrones. In some of these cases (YZ Cas, Pavlovski et al. 2014; EE Peg, Linnell et al. 1996; V1229 Tau, Groenewegen et al. 2007), the slope can be attributed to a low age¹². However, in other cases it is less clear that age or composition can be used to explain the system properties. Among the more important examples:

- BP Vul (Lacy et al. 2003): Both stars in this system show the metal-line phenomenon, and so the bulk composition cannot be inferred from the system itself. However, the stars are close to those of KIC 9777062 in $M - R$ space, and they share a very similar slope in $M - R$ plane. The authors found that the primary star implied a slightly

¹² For V1229 Tau, the system is a member of the Pleiades and can therefore be dated to near 100 Myr. For YZ Cas, the secondary star is of F2 spectral type, and does not show the metal-line phenomenon. Its photospheric composition can therefore constrain the bulk composition of the stars to be near solar.

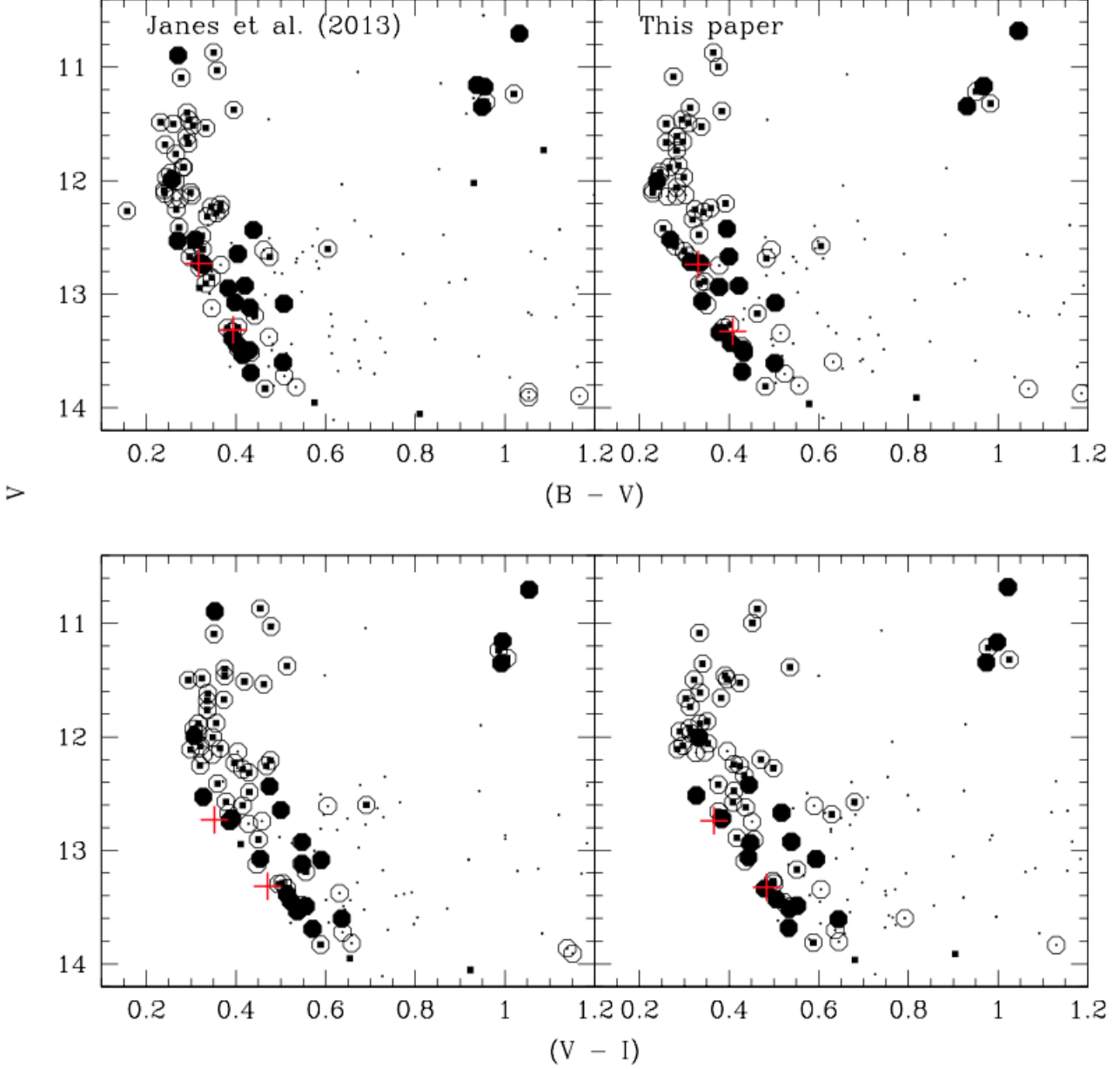


Figure 15. Color-magnitude diagrams for stars in the NGC 6811 field in BV (top row) and VIC (bottom row) from Janes et al. (2013) and this work. Stars with proper motion memberships $P_\mu > 50\%$ in any of the three studies (Sanders 1971; Dias et al. 2002; Kharchenko et al. 2013) are shown with circles, and if proper motion membership is corroborated by radial velocities (Frinchaboy & Majewski 2008; Mermilliod & Mayor 1990; Molenda-Żakowicz et al. 2014; Meibom et al. 2011) the circle is filled. Known or candidate binaries are indicated with small square symbols. The components of KIC 977062 are shown with +.

younger age than the secondary star for a common bulk composition. With the caveat that the bulk composition is not well determined, the inferred age of the system is also quite similar to that of KIC 977062. It should be noted that secondary of BP Vul is one of the least massive stars in this binary star sample showing the Fm phenomenon — no other binary component in the range $1.4 \leq M/M_\odot \leq 1.58$ is known to show metal line anomalies.

- XY Cet (Southworth et al. 2011): This system is composed of two Am stars in a short period (2.78 d) binary, and the secondary star has a mass and radius that are within about 1% of those of the primary of KIC 977062. The bulk composition of the stars cannot be inferred from spectroscopy, but the authors found that the $M - R$ line for the binary was less steep than predicted by any models they used. The best match was to solar abundance models with age near 850 Myr.

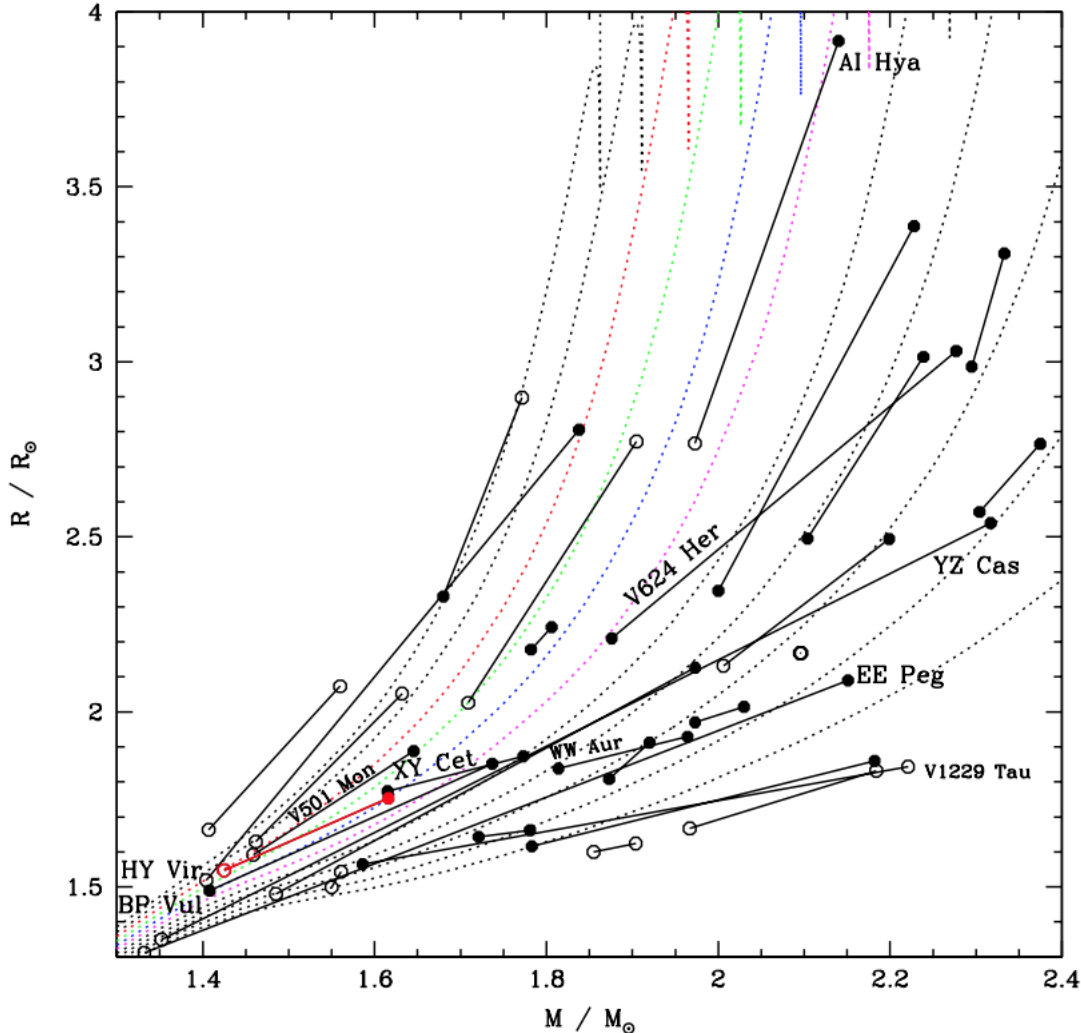


Figure 16. Mass-radius plot for the members of well-studied eclipsing binary stars. Am/Fm stars are shown with solid points, and members of the same binary are connected with line segments. KIC 9777062 is shown in red. PARSEC isochrones with $Z = 0.0137$ and ages between 0.5 and 1.4 Gyr (0.1 Gyr spacing) are shown.

- WW Aur (Southworth et al. 2005): The line segment connecting the stars in this system presents a rather shallow slope that undoubtedly helped push the authors to infer a *highly* super-solar metal abundance and young age (90 Myr). It should be noted that those authors did not see evidence that the Am phenomenon was the cause of the unusual stellar properties.
- Other systems showing shallower slopes in the $M - R$ plane than expected: Al Hya (Popper 1988), V624 Her (Popper 1984), HW CMa (Torres et al. 2012)

Binaries that show this radius discrepancy also appear to show a discrepancy in the relative magnitudes of the two stars, in the sense that the primary star tends to be fainter than expected based on the mass and brightness of the secondary star. KIC 9777062 follows this pattern as well (see §4.2.2).

KIC 9777062 is a valuable addition to the list above because there are constraints on the bulk composition of the stars from both the secondary star and from other stars in the cluster itself. Diffusion is important in the interiors of both stars given that they are both rotating slowly and are massive enough to have mostly radiative envelopes. However, only the primary shows surface heavy element abundances consistent with being a metal-lined star. The lack of δ Sct pulsation from the primary may indicate that helium is draining out of the He II ionization zone that drives the pulsation — a significant fraction of Am stars pulsate, but usually at lower amplitude levels than typical δ Sct stars (Smalley et al. 2011). Models, however, predict that diffusion should result in larger radii (Turcotte et al. 2000) due to increased metal opacity in the surface layers, which runs contrary to what we see in the KIC 9777062 binary. If the Am stars in KIC 9777062 and other binaries are indeed anomalously small in radius, the physical mechanism is still unclear and it is odd that the effect only shows up in some binaries.

- Alam, S., Albareti, F. D., Allende Prieto, C., et al. 2015, *ApJS*, 219, 12
- Allende Prieto, C., Lambert, D. L., Tull, R. G., & MacQueen, P. J. 2002, *ApJL*, 566, L93
- Andersen, J. 1991, *A&A Rev.*, 3, 91
- Asplund, M., Grevesse, N., & Sauval, A. J. 2005, *Cosmic Abundances as Records of Stellar Evolution and Nucleosynthesis*, 336, 25
- Avni, Y. 1976, *ApJ*, 210, 642
- Balona, L. A., Catanzaro, G., Abedigamba, O. P., Ripepi, V., & Smalley, B. 2015, *MNRAS*, 448, 1378
- Balona, L. A., Pigulski, A., Cat, P. D., et al. 2011, *MNRAS*, 413, 2403
- Basu, S., et al. 2011, *ApJL*, 729, L10
- Baumgardt, H., Dettbarn, C., & Wielen, R. 2000, *A&AS*, 146, 251
- Boyajian, T. S., von Braun, K., van Belle, G., et al. 2013, *ApJ*, 771, 40
- Brandt, T. D., & Huang, C. X. 2015, *ApJ*, 807, 58
- Bressan, A., Marigo, P., Girardi, L., et al. 2012, *MNRAS*, 427, 127
- Brogaard, K., Bruntt, H., Grundahl, F., et al. 2011, *A&A*, 525, A2
- Brogaard, K., VandenBerg, D. A., Bruntt, H., et al. 2012, *A&A*, 543, A106
- Brogaard, K., Sandquist, E., Jessen-Hansen, J., Grundahl, F., & Frandsen, S. 2015, *Astrophysics and Space Science Proceedings*, 39, 51
- Brogaard, K., Jessen-Hansen, J., Handberg, R., et al. 2016, *arXiv:1601.01412*
- Brown, T. M., Latham, D. W., Everett, M. E., & Esquerdo, G. A. 2011, *AJ*, 142, 112
- Bruntt, H., Bedding, T. R., Quirion, P.-O., et al. 2010, *MNRAS*, 405, 1907
- Bruntt, H., Deleuil, M., Fridlund, M., et al. 2010, *A&A*, 519, A51
- Bruntt, H., Basu, S., Smalley, B., et al. 2012, *MNRAS*, 423, 122
- Caffau, E., Ludwig, H.-G., Steffen, M., Freytag, B., & Bonifacio, P. 2011, *Sol. Phys.*, 268, 255
- Carquillat, J.-M., Prieur, J.-L., Ginestet, N., Oblak, E., & Kurpinska-Winiarska, M. 2004, *MNRAS*, 352, 708
- Carquillat, J.-M., & Prieur, J.-L. 2007, *MNRAS*, 380, 1064
- Casagrande, L., Ramírez, I., Meléndez, M., & Asplund, M. 2010, *A&A*, 512, A54
- Casagrande, L., & VandenBerg, D. A. 2014, *MNRAS*, 444, 392
- Chaboyer, B., Fenton, W. H., Nelan, J. E., Patnaude, D. J., & Simon, F. E. 2001, *ApJ*, 562, 521
- Charbonneau, P. 1995, *ApJS*, 101, 309
- Claret, A. 2000, *A&A*, 363, 1081
- Coelho, P., Barbuy, B., Meléndez, J., Schiavon, R. P., & Castilho, B. V. 2005, *A&A*, 443, 735
- Corsaro, E., Stello, D., Huber, D., et al. 2012, *ApJ*, 757, 190
- Debosscher, J., Sarro, L. M., López, M., et al. 2009, *A&A*, 506, 519
- Debosscher, J., Blomme, J., Aerts, C., & De Ridder, J. 2011, *A&A*, 529, A89
- Demarque, P., Woo, J.-H., Kim, Y.-C., & Yi, S. K. 2004, *ApJS*, 155, 667
- Dias, W. S., Lépine, J. R. D., & Alessi, B. S. 2002, *A&A*, 388, 168
- Dias, W. S., Monteiro, H., Caetano, T. C., et al. 2014, *A&A*, 564, A79
- Dotter, A. et al. 2008, *ApJS*, 178, 89
- Dravins, D. 1999, *IAU Colloq. 170: Precise Stellar Radial Velocities*, 185, 268
- Dravins, D., & Nordlund, A. 1990, *A&A*, 228, 203
- Eastman, J., Siverd, R., & Gaudi, B. S. 2010, *PASP*, 122, 935
- Everett, M. E., Howell, S. B., & Kinemuchi, K. 2012, *PASP*, 124, 316
- Faigler, S., & Mazeh, T. 2011, *MNRAS*, 415, 3921
- Frandsen, S., & Arentoft, T. 1998, *Journal of Astronomical Data*, 4, 6
- Frinchaboy, P. M., & Majewski, S. R. 2008, *AJ*, 136, 118
- Frinchaboy, P. M., Thompson, B., Jackson, K. M., et al. 2013, *ApJL*, 777, L1
- Gebran, M., Monier, R., Royer, F., Lobel, A., & Blomme, R. 2014, *Putting A Stars into Context: Evolution, Environment, and Related Stars*, 193
- Girardi, L., Mermilliod, J.-C., & Carraro, G. 2000, *A&A*, 354, 892
- Girardi, L., Rubele, S., & Kerber, L. 2009, *MNRAS*, 394, L74
- Glushkova, E. V., Batyrshinova, V. M., & Ibragimov, M. A. 1999, *Astronomy Letters*, 25, 86
- González, J. F., & Levato, H. 2006, *A&A*, 448, 283
- Grevesse, N., Asplund, M., & Sauval, A. J. 2007, *Space Sci. Rev.*, 130, 105
- Groenewegen, M. A. T., Decin, L., Salaris, M., & De Cat, P. 2007, *A&A*, 463, 579
- Gustafsson, B., Edvardsson, B., Eriksson, K., et al. 2008, *A&A*, 486, 951
- Hauschildt, P. H., Baron, E., & Allard, F. 1997, *ApJ*, 483, 390
- Hekker, S., et al. 2011, *A&A*, 530, A100
- Holtzman, J. A., Shetrone, M., Johnson, J. A., et al. 2015, *AJ*, 150, 148
- Honeycutt, R. K. 1992, *PASP*, 104, 435
- Huber, D., Stello, D., Bedding, T. R., et al. 2009, *Communications in Asteroseismology*, 160, 74
- Huber, D., Bedding, T. R., Stello, D., et al. 2011, *ApJ*, 743, 143
- Hut, P. 1981, *A&A*, 99, 126
- Janes, K., Barnes, S. A., Meibom, S., & Hoq, S. 2013, *AJ*, 145, 7
- Kinemuchi, K., Barclay, T., Fanelli, M., et al. 2012, *PASP*, 124, 963
- Kharchenko, N. V., Piskunov, A. E., Schilbach, E., Röser, S., & Scholz, R.-D. 2013, *A&A*, 558, A53
- Kipping, D. M. 2013, *MNRAS*, 435, 2152
- Kwee, K. K., & van Woerden, H. 1956, *Bull. Astron. Inst. Netherlands*, 12, 327
- Lacy, C. H. S., Torres, G., Claret, A., & Sabby, J. A. 2003, *AJ*, 126, 1905
- Landstreet, J. D. 1998, *A&A*, 338, 1041
- Landstreet, J. D., Kupka, F., Ford, H. A., et al. 2009, *A&A*, 503, 973
- Lenz P., Breger M. 2005, *CoAst*, 146, 53
- Linnell, A. P., Hubeny, I., & Lacy, C. H. S. 1996, *ApJ*, 459, 721
- Luo, Y. P., Zhang, X. B., Luo, C. Q., Deng, L. C., & Luo, Z. Q. 2009, *New A*, 14, 584
- Mandel, K., & Agol, E. 2002, *ApJL*, 580, L171
- McNamara, D.H., Clementini, G., & Marconi, M. 2007, *AJ*, 133, 2752
- Meibom, S., Barnes, S. A., Latham, D. W., et al. 2011, *ApJL*, 733, L9
- Meibom, S., Grundahl, F., Clausen, J. V., et al. 2009, *AJ*, 137, 5086
- Meibom, S., Torres, G., Fressin, F., et al. 2013, *Nature*, 499, 55
- Mermilliod, J.-C., & Mayor, M. 1990, *A&A*, 237, 61
- Mermilliod, J.-C., Mayor, M., & Udry, S. 1008, *A&A*, 485, 303
- Mészáros, S., Holtzman, J., García Pérez, A. E., et al. 2013, *AJ*, 146, 133
- Metcalfe, T. S. 1999, *AJ*, 117, 2503
- Miglio, A., Brogaard, K., Stello, D., et al. 2012, *MNRAS*, 419, 2077
- Molenda-Żakowicz, J., Brogaard, K., Niemczura, E., et al. 2014, *MNRAS*, 445, 2446
- Molenda-Żakowicz, J., Sousa, S. G., Frasca, A., et al. 2013, *MNRAS*, 434, 1422
- Munari, U., & Zwitter, T. 1997, *A&A*, 318, 269
- Murphy, S. J., Shibahashi, H., & Kurtz, D. W. 2013, *MNRAS*, 430, 2986
- Murphy, S. J., Bedding, T. R., Shibahashi, H., Kurtz, D. W., & Kjeldsen, H. 2014, *MNRAS*, 441, 2515.
- Netopil, M., Paunzen, E., Maitzen, H. M., North, P., & Hubrig, S. 2008, *A&A*, 491, 545
- Niemczura, E., Murphy, S. J., Smalley, B., et al. 2015, *MNRAS*, 450, 2764
- Orosz, J. A., Groot, P. J., van der Klis, M., et al. 2002, *ApJ*, 568, 845
- Orosz, J. A., & Hauschildt, P. H. 2000, *A&A*, 364, 265
- Pamyatnykh, A. A. 2000, *Delta Scuti and Related Stars*, 210, 215
- Pavlovski, K., Southworth, J., Kolbas, V., & Smalley, B. 2014, *MNRAS*, 438, 590
- Peña, J. H., Fox Machado, L., García, H., et al. 2011, *Rev. Mexicana Astron. Astrofis.*, 47, 309
- Popper, D. M. 1984, *AJ*, 89, 1057
- Popper, D. M. 1988, *AJ*, 95, 190
- Prša, A., et al. 2011, *AJ*, 141, 83
- Ramírez, I., & Meléndez, J. 2005, *ApJ*, 626, 465
- Rentzsch-Holm, I. 1996, *A&A*, 312, 966
- Richer, J., Michaud, G., & Turcotte, S. 2000, *ApJ*, 529, 338
- Rose, M. B., & Hintz, E. G. 2007, *AJ*, 134, 2067

- Rucinski, S. M. 1992, *AJ*, 104, 1968
- Ryabchikova, T., Piskunov, N., Kurucz, R. L., et al. 2015, *Phys. Scr.*, 90, 054005
- Sandberg Lacy, C. H., & Fekel, F. C. 2011, *AJ*, 142, 185
- Sanders, W. L. 1971, *A&A*, 15, 368
- Sandquist, E. L., Latham, D. W., Shetrone, M. D., & Milone, A. A. E. 2003, *AJ*, 125, 810
- Sandquist, E. L., Mathieu, R. D., Brogaard, K., et al. 2013, *ApJ*, 762, 58
- Schlafly, E. F., & Finkbeiner, D. P. 2011, *ApJ*, 737, 103
- Sharma, S., Stello, D., Bland-Hawthorn, J., Huber, D., & Bedding, T. R. 2016, *ApJ*, 822, 15
- Shetrone, M., et al. 2007, *PASP*, 119, 556
- Shibahashi, H., & Kurtz, D. W. 2012, *MNRAS*, 422, 738
- Skrutskie, M. F. et al. 2006, *AJ*, 131, 1163
- Slawson, R. W., Prša, A., Welsh, W. F., et al. 2011, *AJ*, 142, 160
- Smalley, B., Kurtz, D. W., Smith, A. M. S., et al. 2011, *A&A*, 535, A3
- Smith, J. C., Stumpe, M. C., Van Cleve, J. E., et al. 2012, *PASP*, 124, 1000
- Southworth, J., Smalley, B., Maxted, P. F. L., Claret, A., & Etzel, P. B. 2005, *MNRAS*, 363, 529
- Southworth, J., Pavlovski, K., Tamajo, E., et al. 2011, *MNRAS*, 414, 3740
- Stello, D., Huber, D., Kallinger, T., et al. 2011, *ApJ*, 737, L10
- Stello, D., Meibom, S., Gilliland, R. L., et al. 2011, *ApJ*, 739, 13
- Stetson, P. B. 1987, *PASP*, 99, 191
- Stetson, P. B. 1990, *PASP*, 102, 932
- Stetson, P. B. 2000, *PASP*, 112, 925
- Stumpe, M. C., Smith, J. C., Van Cleve, J. E., et al. 2012, *PASP*, 124, 985
- Suárez, J. C., García Hernández, A., Moya, A., et al. 2014, *A&A*, 563, AA7
- Szentgyorgyi, A., Furesz, G., Cheimets, P., et al. 2011, *PASP*, 123, 1188
- Tegmark, M., Strauss, M. A., Blanton, M. R., et al. 2004, *Phys. Rev. D*, 69, 103501
- Telting, J. H., Avila, G., Buchhave, L., et al. 2014, *AN*, 335, 41
- Tkachenko, A., Aerts, C., Yakushechkin, A., et al. 2013, *A&A*, 556, A52
- Torres, G., Lacy, C. H., Marschall, L. A., Sheets, H. A., & Mader, J. A. 2006, *ApJ*, 640, 1018
- Torres, G., Andersen, J., & Giménez, A. 2010, *A&A Rev.*, 18, 67
- Torres, G., Clausen, J. V., Bruntt, H., et al. 2012, *A&A*, 537, A117
- Torres, G., Sandberg Lacy, C. H., Pavlovski, K., Fekel, F. C., & Muterspaugh, M. W. 2015, *AJ*, 150, 154
- Tull, R. G. 1998, *Proc. SPIE*, 3355, 387
- Turcotte, S., Richer, J., & Michaud, G. 1998, *ApJ*, 504, 559
- Turcotte, S., Richer, J., Michaud, G., & Christensen-Dalsgaard, J. 2000, *A&A*, 360, 603
- Uytterhoeven, K., Moya, A., Grigahcène, A., et al. 2011, *A&A*, 534, A125
- van Cauteren, P., Lampens, P., Robertson, C. W., & Strigachev, A. 2005, *Communications in Asteroseismology*, 146, 21
- VandenBerg, D. A., Bergbusch, P. A., & Dowler, P. D. 2006, *ApJS*, 162, 375
- VandenBerg, D. A., & Clem, J. L. 2003, *AJ*, 126, 778
- Wilson, J. C., Hearty, F., Skrutskie, M. F., et al. 2010, *Proc. SPIE*, 7735, 77351C
- Yang, W., Meng, X., & Li, Z. 2010, *MNRAS*, 409, 873
- Yontan, T., Bilir, S., Bostancı, Z. F., et al. 2015, *Ap&SS*, 355, 267
- Zahn, J.-P. 1975, *A&A*, 41, 329
- Zacharias, N., Finch, C. T., Girard, T. M., et al. 2013, *AJ*, 145, 44

Table 8
Giant Stars in the NGC 6811 Field

Identifications ^a :	9409513 G53	9716522 170 5441 2634	9776739 140 4726 118	9532903 194	9655101 95 3278 530	9534041 G47	9655167 106 3603	9716090 92 3202 2356	9897838 G59
α (2000)	19:36:04.25	19:37:34.62 ^c	19:37:22.07	19:37:50.18	19:36:57.13	19:39:32.94	19:37:02.68	19:36:55.81	19:38:31.12
δ (2000)	+45:58:27.5	+46:24:09.9 ^c	+46:32:50.6	+46:07:46.5	+46:22:42.6	+46:11:55.4	+46:23:13.1	+46:27:37.7	+46:47:33.3
Photometry:									
V	10.543 ± 0.033	10.703 ± 0.018	11.157 ± 0.015	11.165 ± 0.002	11.235 ± 0.016	11.272 ± 0.016	11.306 ± 0.003	11.350 ± 0.006	11.142 ± 0.001
$B - V$	0.952 ± 0.007	1.032 ± 0.009	0.938 ± 0.007	0.968 ± 0.003	1.020 ± 0.083	0.930 ± 0.019	0.958 ± 0.001	0.949 ± 0.016	0.857 ± 0.025
$V - I$	1.054 ± 0.005	1.054 ± 0.005	0.995 ± 0.002	0.998 ± 0.004	0.986 ± 0.002	0.930 ± 0.019	1.005 ± 0.002	0.992 ± 0.002	
$V - K_s$	2.297 ± 0.035	2.440 ± 0.023	2.23 ± 0.019	2.264 ± 0.012	2.241 ± 0.019	2.202 ± 0.021	2.287 ± 0.011	2.264 ± 0.013	2.191 ± 0.011
$T_{\text{eff}}^{\text{d}}$ (K)	4950	4805	5025	4990	5010	5060	4960	4990	
$T_{\text{eff}}^{\text{e}}$ (K)	5065	4952	4952	5105	5111	5107	5091	4980	
$T_{\text{eff}}^{\text{f}}$ (K)				5008	5005		4924		
[Fe/H] ^e	0.10 ± 0.03	0.04 ± 0.03		0.02 ± 0.03	-0.03 ± 0.03	-0.03 ± 0.03	-0.01 ± 0.03		
$\Delta\nu$ (μHz)	6.044 ± 0.026	4.856 ± 0.019	7.621 ± 0.032	7.548 ± 0.029	7.871 ± 0.023	8.375 ± 0.026	8.040 ± 0.033	8.519 ± 0.035	
ν_{max} (μHz)	70.69 ± 0.97	54.10 ± 1.08	94.86 ± 2.29	93.15 ± 1.81	98.71 ± 2.64	108.94 ± 1.85	105.33 ± 5.97	109.68 ± 2.47	
M (M_{\odot})	2.29 ± 0.12	2.35 ± 0.16	2.24 ± 0.18	2.18 ± 0.15	2.21 ± 0.19	2.35 ± 0.14	2.43 ± 0.42	2.19 ± 0.17	
R (R_{\odot})	10.45 ± 0.20	12.20 ± 0.29	8.88 ± 0.24	8.86 ± 0.21	8.65 ± 0.25	8.47 ± 0.18	8.81 ± 0.51	8.19 ± 0.21	
Membership:									
S71		97	97	97	97		97	94	
UCAC4	36	99	99	99	99	99	99	99	0
K13	27	93	87	83	17	13	22	95	0
RV	Y	Y	Y	Y	B	Y	B	Y	Y
Seismic	?	Y	Y	Y	Y	Y	Y	Y	N
Position	N	Y	Y	N	Y	N	Y	Y	N
Notes:	AGB? binary?	AGB	RC	RC	RC, SBI?	RC?	RC, SBI	RC	nonmem.

^a S71: Sanders (1971); J13: Janes et al. (2013); G99: Glushkova et al. (1999); UCAC4: Zacharias et al. (2013), Dias et al. (2014); K13: Kharchenko et al. (2013).

^b Full *Tycho* ID is TYC 3556-XXXXX-1.

^c Incorrect position given in SIMBAD and Mermilliod et al. (2008).

^d from $V - K_s$ color using Ramirez & Meléndez (2005) relations with $E(B - V) = 0.07$.

^e from APOGEE (Data Release 12).

^f from Molenda-Żakowicz et al. (2014).

Table 9
Pulsating Main Sequence Stars in the NGC 6811 Field

S71	Identifications ^a		Position			Photometry		Membership ^a				Notes ^c	
	J13	Tycho ^b	α (2000)	δ (2000)	V	$B - V$	$V - I$	S71	UCAC4	K13	RV		Pos
108	3636	1668	19:37:03.23	+46:19:25.7	10.869 ± 0.012	0.350 ± 0.016	0.454 ± 0.002	96	99	78	B	Y	δ Sct (vC,L,U,D); 1
205	6724	1676	19:37:58.76	+46:14:19.4	11.028 ± 0.014	0.358 ± 0.016	0.478 ± 0.002	89	99	87	B	N	δ Sct (vC,L,D); 2
136 ^d	4690	1768	19:37:21.48	+46:24:33.8	11.092 ± 0.004	0.278 ± 0.002	0.351 ± 0.002	96	99	87	B	Y	δ Sct (vC,L); 3
86	2988	1838	19:36:51.91	+46:23:20.4	11.400 ± 0.011	0.291 ± 0.007	0.375 ± 0.211	97	99	66	B	Y	δ Sct (D,U)
75	2456	9532168	19:36:47.21	+46:09:48.8	11.41	0.24		60	99	90	B	N	δ Sct (B); 3
166	5314	1698	19:37:32.10	+46:19:15.0	11.464 ± 0.013	0.295 ± 0.006	0.375 ± 0.003	93	99	19 ^e	B	Y	δ Sct (vC,L,U), 4
87	3004	2336	19:36:52.01	+46:32:05.1	11.484 ± 0.003	0.232 ± 0.023	0.324 ± 0.003	97	99	81	B	Y	δ Sct (B); 5
144	4845	716	19:37:24.09	+46:23:52.1	11.512 ± 0.014	0.304 ± 0.008	0.419 ± 0.003	54	99	98	B	Y	δ Sct (vC,L,U,D)
121	4249	2492	19:37:13.77	+46:25:25.7	11.618 ± 0.007	0.290 ± 0.009	0.337 ± 0.003	96	99	52	N	Y	B variable (B)
149	4946	9655444	19:37:25.64	+46:18:36.8	11.671 ± 0.007	0.294 ± 0.008	0.373 ± 0.003	95	99	0	B	Y	δ Sct (D)
127	4453	856	19:37:17.10	+46:23:14.7	11.763 ± 0.007	0.266 ± 0.007	0.336 ± 0.003	93	99	91	B	Y	EW with δ Sct; 6
9909	3387	9595743	19:39:19.22	+46:14:57.5	11.812 ± 0.008	0.319 ± 0.005	0.393 ± 0.003	0	0	0	0	N	7
113	3765	1344	19:37:05.46	+46:24:58.5	11.879 ± 0.007	0.282 ± 0.005	0.356 ± 0.003	95	99	63	B	Y	δ Sct (L,D,B)
230	7342	1690	19:38:16.13	+46:31:31.9	11.930 ± 0.008	0.254 ± 0.002	0.306 ± 0.040	97	99	97	B	N	hybrid; 8
157	5067	1888	19:37:27.79	+46:23:10.1	12.003 ± 0.009	0.265 ± 0.013	0.348 ± 0.002	96	99	72	B	Y	δ Sct (L,D)
192	6195	914	19:37:48.08	+46:27:25.3	12.082 ± 0.011	0.240 ± 0.003	0.321 ± 0.008	92	99	99	B	Y	δ Sct (D); 9
97	3339	944	19:36:58.21	+46:20:23.9	12.101 ± 0.024	0.299 ± 0.028	0.365 ± 0.003	97	99	86	B	Y	δ Sct (vC,L,U,B); 10
206	6846	2232	19:38:01.74	+46:19:07.0	12.131 ± 0.004	0.301 ± 0.001	0.404 ± 0.003	94	99	93	0	Y	δ Sct (D)
146	4896	9655433	19:37:24.86	+46:18:39.0	12.159 ± 0.005	0.260 ± 0.007	0.326 ± 0.003	96	87	0	0	Y	δ Sct (B); 11
219	7013	382	19:38:06.73	+46:36:30.7	12.208 ± 0.005	0.366 ± 0.007	0.477 ± 0.006	0	12	61	B	N	δ Sct (D); 10
195	6335	370	19:37:50.59	+46:35:23.2	12.230 ± 0.008	0.345 ± 0.011	0.397 ± 0.004	93	99	30	Y	N	γ Dor; 12
81	2852	2038	19:36:49.68	+46:14:26.3	12.252 ± 0.006	0.267 ± 0.014	0.320 ± 0.004	89	99	0	B	Y	δ Sct (D,B)
147	4918	9655438	19:37:25.23	+46:19:35.7	12.255 ± 0.006	0.365 ± 0.003	0.468 ± 0.003	97	99	91	B	Y	hybrid (U); 8, 10
115	3998	9716256	19:37:09.67	+46:27:09.0	12.273 ± 0.013	0.319 ± 0.003	0.403 ± 0.002	0	0	0	Y	Y	γ Dor; 8
138	4735	1762	19:37:22.18	+46:18:51.2	12.286 ± 0.041	0.356 ± 0.051	0.415 ± 0.003	0	73	46	B	Y	δ Sct (D); 10
165	5258	1248	19:37:31.22	+46:21:32.0	12.411 ± 0.007	0.273 ± 0.010	0.359 ± 0.003	93	99	43	B	Y	δ Sct (D), hybrid (U)
143	4818	9655419	19:37:23.63	+46:23:26.7	12.486 ± 0.004	0.324 ± 0.005	0.430 ± 0.003	90	99	50	B	Y	δ Sct (L,D)
169	5377	306	19:37:33.59	+46:37:08.8	12.528 ± 0.011	0.270 ± 0.019	0.327 ± 0.018	95	99	30	B	N	δ Sct (L,D)
255	8365	3564	19:38:41.15	+46:07:01.4	12.549 ± 0.009	0.390 ± 0.012		0	0	0	N	N	SPB (D)
135	4687	9655393	19:37:21.37	+46:19:53.3	12.571 ± 0.005	0.299 ± 0.008	0.378 ± 0.003	94	99	84	Y	Y	δ Sct (L,U,B); 8
201	6501	9655800	19:37:53.16	+46:18:28.8	12.644 ± 0.010	0.400 ± 0.009	0.500 ± 0.004	94	99	70	Y	Y	γ Dor (U,D)
119	4182	9655288	19:37:12.44	+46:23:29.3	12.672 ± 0.005	0.297 ± 0.008	0.384 ± 0.003	95	14	23	B	Y	δ Sct (L,D)
272		9777807	19:38:54.91	+46:33:47.7	12.728	0.345		47	99	60	N	N	γ Dor (D)
142	4772	9655407	19:37:22.74	+46:22:53.9	12.742 ± 0.007	0.366 ± 0.013	0.458 ± 0.003	96	99	85	Y	Y	δ Sct (D)
101	3464	9776474	19:37:00.19	+46:31:14.2	12.765 ± 0.019	0.319 ± 0.017	0.428 ± 0.004	96	99	37	Y	Y	δ Sct (U)
152		9532644	19:37:26.47	+46:10:07.7	12.786	0.350		96	99	47	N	N	hybrid (U)
646		9836020	19:35:43.13	+46:40:02.7	12.799 ± 0.004	0.346 ± 0.005		94	91	Y	Y	N	δ Sct (U)
256	8386	9533489	19:38:41.70	+46:07:21.6	12.854 ± 0.001	0.346 ± 0.002		97	97	46	B	N	hybrid (U); 13
162	5171	9776816	19:37:29.69	+46:30:39.6	12.904 ± 0.008	0.333 ± 0.015	0.450 ± 0.015	96	10	34	B	Y	γ Dor (U,D)
4962		9897089	19:37:25.98	+46:43:54.2	12.945 ± 0.008	0.319 ± 0.016	0.411 ± 0.001	92	98	63	B	N	δ Sct (D)
225	7201	9716947	19:38:11.95	+46:28:02.5	12.947 ± 0.005	0.383 ± 0.008		92	99	83	Y	Y	hybrid (U)
27	772	9836073	19:35:48.42	+46:37:29.9	12.994 ± 0.002	0.341 ± 0.002		34	99	74	Y	N	δ Sct?, misc (D)
94	3259	9716107	19:36:56.76	+46:26:58.0	13.073 ± 0.012	0.398 ± 0.072	0.454 ± 0.004	95	96	79	Y	Y	γ Dor (U)
91	3208	9410527	19:37:30.25	+45:56:52.3	13.110	0.397		99	99	15	Y	Y	γ Dor (D)
171	5442	9594100	19:36:55.99	+46:15:18.5	13.118 ± 0.077	0.431 ± 0.003		93	99	58	Y	Y	γ Dor (U)
102	3514	9716523	19:37:34.64	+46:26:01.9	13.124 ± 0.021	0.346 ± 0.023	0.447 ± 0.008	96	84	0	0	Y	γ Dor (D)
137	4724	9655151	19:37:01.18	+46:22:59.4	13.290 ± 0.005	0.404 ± 0.016	0.504 ± 0.004	97	95	65	B	Y	γ Dor (U)
137	4724	9655399	19:37:22.00	+46:20:50.5	13.297 ± 0.002	0.381 ± 0.001	0.495 ± 0.004	97	87	21	B	Y	γ Dor
51	1841	9654789	19:36:28.80	+46:18:39.2	13.333 ± 0.007	0.392 ± 0.023	0.513 ± 0.006	94	98	61	B	Y	γ Dor (U,D)
79		9594007	19:36:48.86	+46:14:29.4	13.386	0.371		96	91	0	0	Y	γ Dor; 14
131	4505	9716350	19:37:17.98	+46:27:45.2	13.387 ± 0.009	0.392 ± 0.013	0.514 ± 0.020	95	94	0	Y	Y	γ Dor; 15
209	6897	9594915	19:38:02.88	+46:17:22.5	13.639 ± 0.010	0.387 ± 0.009	0.522 ± 0.007	0	91	24	Y	Y	δ Sct (vC,L); 16

^a S71: Sanders (1971); J13: James et al. (2013); UCAC4: Zacharias et al. (2013), Dias et al. (2014); K13: Kharchenko et al. (2013).

^b Full *Tycho* ID is TYC 3556-XXXX-1.

^c Variability identifications from B: Balona et al. (2011); T: Tkachenko et al. (2013); U: Uytterhoeven et al. (2011); vC: van Cauwtere et al. (2005); L: Luo et al. (2009). Square brackets indicate earlier identifications we believe are incorrect. 1) binary? 2) SBI? On blue hook? 3) [misc. (D)]. 4) HIP96532. 5) [β Cep (D)]; long P binary. 6) [misc./rot. (D)]. 7) γ Dor (T), SPB (D), 8) [β Cep (D)]. 9) SBI. 10) Redward of MS. 11) Suspected binary? 12) EB. 13) EB ($P = 197.146$ d). 14) [SPB (D)]. 15) [rotation/activity (U)].

Table 10
Miscellaneous Bright Stars in the NGC 6811 Field

S71	Identifications ^a		Position		δ (2000)	V	Photometry		V - I	S71	Membership ^a		Pos	Notes ^c
	J13	Tycho ^b	α (2000)	KIC			B - V	UCAC4			K13	RV		
247	7930	3228	19:38:31.06	9777532	+46:31:34.1	10.894 ± 0.010	0.271 ± 0.007	0.352 ± 0.002	97	99	50	Y	N	1
172	5459	1874	19:37:34.98	9655543	+46:20:53.8	11.375 ± 0.015	0.395 ± 0.008	0.514 ± 0.002	97	99	67 ^d	B	Y	2
110	3699	1396	19:37:04.21	9655187	+46:18:07.8	11.499 ± 0.009	0.260 ± 0.009	0.294 ± 0.003	97	99	97	B	Y	EB; 3
161	5148	1414	19:37:29.26	9716465	+46:29:21.6	11.536 ± 0.008	0.333 ± 0.008	0.462 ± 0.002	64	99	40	B	Y	4
188	5968	882	19:37:43.64	9716628	+46:29:50.5	11.681 ± 0.003	0.242 ± 0.004	0.336 ± 0.001	97	99	30	B	Y	4, 5
77	2772	1100	19:36:48.16	9655005	+46:19:38.0	11.883 ± 0.008	0.283 ± 0.011	0.316 ± 0.003	97	99	85	B	Y	4, 5, 6
159	5112	9716456	19:37:28.53	9716456	+46:24:18.3	11.970 ± 0.012	0.245 ± 0.015	0.316 ± 0.003	97	99	89	B	Y	EB; 7
134	4602	1352	19:37:19.77	9655382	+46:20:55.3	11.992 ± 0.008	0.257 ± 0.009	0.307 ± 0.002	88	99	30	Y	Y	4, 5
189	6025	2272	19:37:44.78	9716637	+46:25:01.0	12.111 ± 0.006	0.241 ± 0.008	0.299 ± 0.003	97	99	99	B	Y	8
103	3534	9655155	19:37:01.59	9655155	+46:20:25.7	12.158 ± 0.011	0.275 ± 0.004	0.347 ± 0.003	90	99	37	B	Y	5
46	1457	2536	19:36:18.60	9531823	+46:09:43.5	12.266 ± 0.005	0.157 ± 0.007		66	99	16	B	N	9, 10
118	4151	9532445	19:37:12.12	9532445	+46:10:13.0	12.519 ± 0.005	0.309 ± 0.006		96	99	65	Y	N	5
100	3453	9716154	19:37:00.03	9716154	+46:25:21.1	12.600 ± 0.022	0.605 ± 0.009	0.691 ± 0.004	57	99	58	B	Y	9, 11
123	4284	9655312	19:37:14.26	9655312	+46:18:57.2	12.741 ± 0.011	0.328 ± 0.011	0.386 ± 0.003	97	99	24	Y	Y	4, 5
158	5074	9655471	19:37:27.91	9655471	+46:22:26.6	13.600 ± 0.003	0.505 ± 0.001	0.636 ± 0.004	96	95	46	Y	Y	9
8746		9656397	19:38:50.23	9656397	+46:23:05.0	13.953 ± 0.007	0.575 ± 0.018	0.654 ± 0.007		98		Y	N	EB, 12
3418		9655129	19:36:59.55	9655129	+46:22:26.4	14.054 ± 0.032	0.810 ± 0.012	0.923 ± 0.004		72	1		Y	EB, 13
6630		9837544	19:37:56.73	9837544	+46:40:34.1	15.463 ± 0.003	0.988 ± 0.003	1.098 ± 0.006		94	77		N	EB, 14

^a S71: Sanders (1971); J13: Janes et al. (2013); UCAC4: Zacharias et al. (2013); Dias et al. (2014); K13: Kharchenko et al. (2013).

^b Full *Tycho* ID is TYC 3556-XXXXX-1.

^c Variability identifications from B: Balona et al. (2011); D: Debosscher et al. (2011); U: Uytterhoeven et al. (2011); vC: van Cauteren et al. (2005). 1) rotation/activity (U). 2) HIP96538. 3) $P = 4.4177$ d. 4) misc. (D). 5) rot. (B). 6) 1.5d variations. 7) $P = 1.81329$ d. 8) no obvious pulsation. 9) act. (D). 10) odd light curve. 11) nonmember or triple? 12) $P = 204.471$ d. 13) $P = 2.74405$ d; nonmember? 14) $P = 71.6619$ d.

^d Also identified as proper motion member in Baumgardt et al. (2000).